

# Reactivity-informed design, synthesis, and Michael addition kinetics of C-ring andrographolide analogs

Alice Zhou<sup>1,2</sup>, Warren Chang<sup>1,3</sup>, Tiffany Wang<sup>1,4</sup>, Jeslyn Wu<sup>1,3</sup>, Selin Kocalar<sup>1,5</sup>, Lakshman Swaminathan<sup>1,6</sup>, Aishi Rao<sup>1,3</sup>, Samyukta Athreya<sup>1,7</sup>, Priya Chanda<sup>1,8</sup>, Edward Njoo<sup>1</sup>

<sup>1</sup> Department of Chemistry, Biochemistry & Physics, Aspiring Scholars Directed Research Program, Fremont, California

<sup>2</sup> BASIS independent Silicon Valley, San Jose, California

<sup>3</sup> Mission San Jose High School, Fremont, California

<sup>4</sup> Saratoga High School, Saratoga, California

<sup>5</sup> Leigh High School, San Jose, California

<sup>6</sup> Amador Valley High School, Pleasanton, California

<sup>7</sup> American High School, Fremont, California

<sup>8</sup> Irvington High School, Fremont, California

## SUMMARY

Andrographolide, a labdane diterpenoid lactone natural product extracted from *Andrographis paniculata*, has demonstrated potent biological activity and therapeutic potential against cancer, Alzheimer's disease, diabetes, and multiple sclerosis. Andrographolide is reported to significantly inhibit the NF- $\kappa$ B signaling pathway, which is active in immune system function and regulation of inflammatory cells. However, andrographolide use is not optimized for human systems. In order to improve upon these aspects, we designed and semi-synthesized a library of andrographolide analogues with modified electronics of the 12,13 unsaturated lactone to increase cytotoxicity via the addition of electron-withdrawing groups, thereby influencing reactivity of the compound. Reactivity of the top piece butenolide warhead was quantified via a time-resolved colorimetric *ex vivo* Michael addition assay using Elleman's Method, wherein reduced-glutathione was the electron donor. The results demonstrate that the installation of an acetate ester at C14 did not result in greater Michael acceptor reactivity, whereas changing the electrophile to C14 with a C11-C12 alkene resulted in a significantly higher rate of reaction with glutathione. Further, computational studies were employed to model the Michael addition energetic pathways of andrographolide and each analog. We found the energetic pathways for all analogs were relatively consistent, suggesting that changes in sterics may play a more significant role in defining Michael addition kinetics. Through understanding the kinetic mechanisms of the Michael acceptor pharmacophore in andrographolide, we hope to further inform directed semisyntheses in order to optimize this incredibly potent natural product for clinical use.

## INTRODUCTION

Andrographolide, a labdane diterpenoid lactone natural product isolated from the plant *Andrographis paniculata*, has received much attention for its diverse biological activity, including its anti-cancer, anti-diabetic, anti-inflammatory, anti-bacterial, antiviral, and anti-malarial properties (1–9) (Figure 1a). This compound primarily exerts its activity by covalently modifying NF- $\kappa$ B, a transcription factor that lies at the crossroads of numerous biological pathways, particularly those involved in inflammation, mechanotransduction, and cell survival (10, 11). Additionally, andrographolide has been shown to modulate cell proliferation and apoptosis through interference in pathways including p27, caspase, and COX-2 expression (12–15). This natural product's diverse mechanisms of biological activity have made it a high-

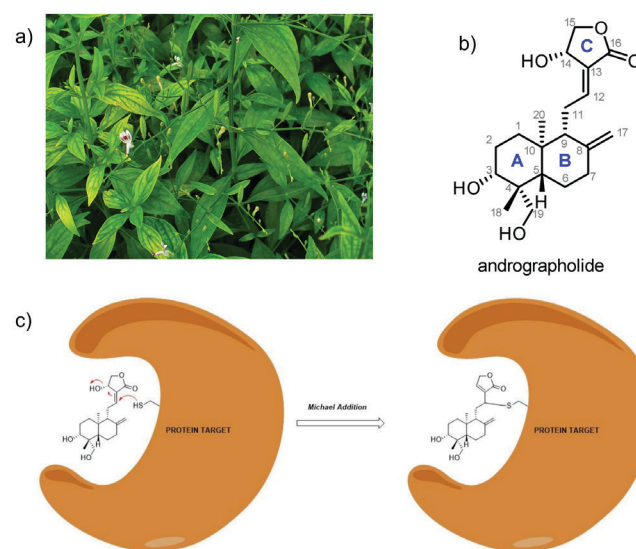


**Figure 1: The structure and mechanism of action of andrographolide, a labdane diterpenoid natural product.** a) Structure of andrographolide, a natural product which is isolated from the leaves of the plant *Andrographis paniculata*. b) Schematic of Michael addition between andrographolide and cysteine residues on protein targets.

potential candidate for the development of biomedical drugs (16).

Andrographolide derives its ability to modulate various cellular pathways from its general role as a Michael acceptor, or electrophile (17). The Michael acceptor on andrographolide is the C-12 position, at which this natural product contains an  $\alpha,\beta$ -unsaturated carbonyl, which can irreversibly and covalently bind to cysteine residues on protein targets (18) (**Figure 1b**). Most notably, andrographolide is able to form a covalent adduct to Cysteine-62 of the p50 subunit on the transcription factor NF- $\kappa$ B, through which it exerts its most significant biological impacts (19). Already, andrographolide has been involved in multiple clinical trials, including a trial where it diminished brain atrophy and was demonstrated to be well-tolerated in patients diagnosed with multiple sclerosis, as well as another trial that showed it inhibited HIV-induced cell cycle dysregulation (20–22). Although this natural product is readily isolated from phytochemical sources and presents a great deal of therapeutic potential itself, semi-synthetic derivatives of andrographolide can be optimized for greater performance (23). Currently, synthetic compounds inspired by natural products outnumber natural products in clinical use five to one; this has indeed been the case in a number of modern cancer drugs inspired by or semi-synthetically derived from natural products, including Topotecan and Docetaxel (24–27).

We hypothesized that structural modification of andrographolide through chemical semi-synthesis may lead to the identification of analogs with greater biological activity. In particular, we investigated how structural modification of the 12,13-unsaturated lactone C-ring fragment may alter the stereoelectronics of the Michael acceptor warhead. By altering the Michael acceptor, we expected to see changes in the

compounds' Michael addition kinetics and biological activity. Previous studies demonstrated that installments of electron-withdrawing groups at C-14 result in greater cytotoxicity (28). Additionally, 14-deoxy-11,12-didehydroandrographolide and 14-deoxy-14,15-didehydroandrographolide, which are andrographolide analogs isolated from the same plant, have shown greater anti-cancer activity.

Here, we present the semi-synthesis and biochemical evaluation of andrographolide and four semi-synthetic derivatives. We found that the relative reactivity of these compounds as Michael acceptor electrophiles could be evaluated in an *ex vivo* colorimetric Michael addition assay using glutathione, a commercially available tripeptide that might serve as a proxy for more generalized reactivity against protein targets with thiol nucleophiles, including NF- $\kappa$ B. Moreover, the thermodynamic basis for trends observed in reactivity was modeled quantum mechanically by density-functional theory (DFT) free energy calculations.

We hypothesized that enhanced the Michael acceptor reactivity of the analogs are directly related to increased electron-withdrawing capabilities of the substituents at C14 on andrographolide, such as installation of an acetate ester (Compound 3). Additionally, since the 14-deoxy-11,12-didehydroandrographolide and 14-deoxy-14,15-didehydroandrographolide have already been demonstrated to show amplified biological effects, we expected to observe faster Michael addition kinetics from them. We found that sterics, rather than electronics, are more influential in the reaction kinetics of the C-ring diversified compounds, and hope that this finding may direct further endeavors in optimizing the therapeutic potential of andrographolide derivatives.

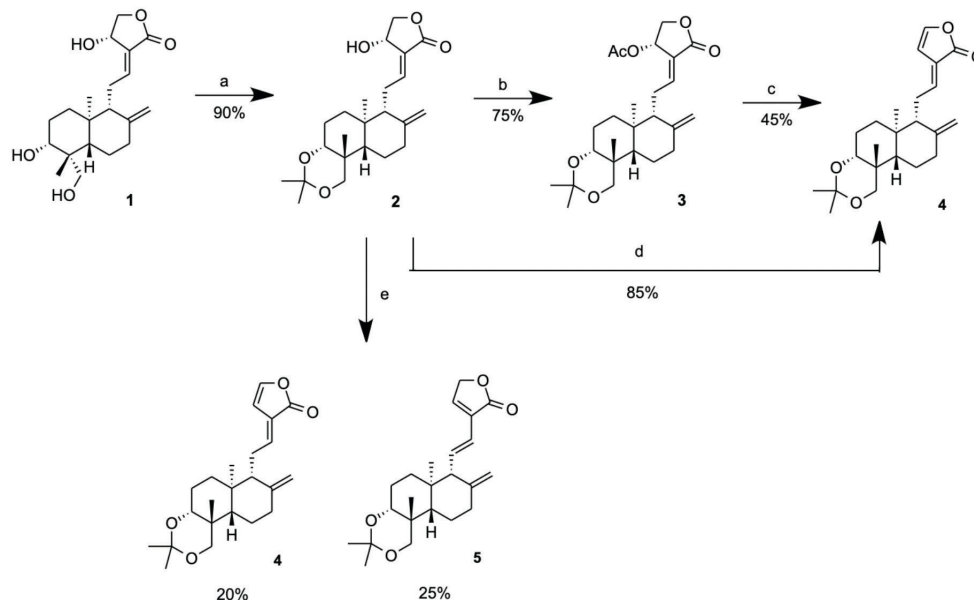


**Figure 2: Synthesis of andrographolide analogs.** a) 2,2-dimethoxypropane, PPTS, acetone, r.t., 30 min. b) Ac<sub>2</sub>O, 80 °C, 2 hr. c) Et<sub>3</sub>N, DCM, r.t., 1 hr.; d) Ac<sub>2</sub>O, DMAP, Et<sub>3</sub>N, DCM, r.t., 2 hr. e) PhNTf<sub>2</sub>, DBU, MeCN, r.t., 15 min.

## RESULTS

### Chemical Synthesis

Herein, four andrographolide derivatives (Compounds **2-5**) were semi-synthesized (**Figure 2**). Our efforts began with acetonide protection of the 1,3-diol system at C-3 and C-19 on andrographolide which was accomplished with 2,2 dimethoxypropane and catalytic pyridinium p-toluene sulfonate (PPTS) in anhydrous acetone (dried over molecular sieves prior to use), which gave acetonide (Compound **2**) in high yields. Consistent with previous reports, treatment of acetonide (Compound **2**) with refluxing acetic anhydride gave

the corresponding C-14 acetate (Compound **3**) (**29**). We also found that addition of base to the C-14 acetate **3** led to the C-14 C-15 eliminated product **4**. Previously, elimination product **5** has been co-isolated as a minor product in the treatment of acetonide (Compound **2**) with 4-dimethylaminopyridine (DMAP) (**30**). However, we found that treating compound **2** with N-phenyl triflate (PhNTf<sub>2</sub>) and 1,8-diazabicyclo[5.4.0]undec-7-ene (DBU) resulted in elimination of the C14 hydroxy group almost instantaneously, with quantitative conversion by <sup>19</sup>F nuclear magnetic resonance (NMR) spectroscopy (**Figure 3**). Compounds **4** and **5** were chromatographically

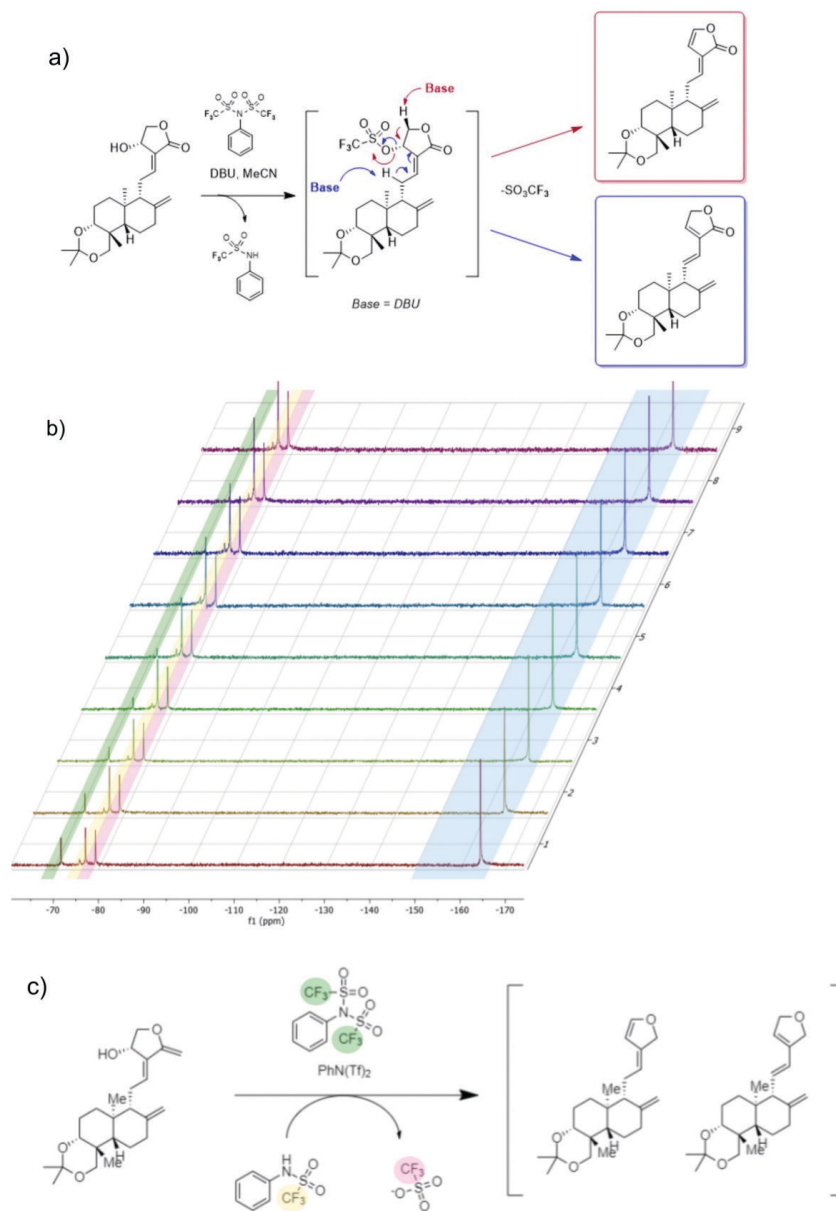


**Figure 3:** <sup>19</sup>F nuclear magnetic resonance (NMR) spectroscopy enables real-time monitoring of a tandem triflation-elimination sequence. a) Putative reaction mechanism for the formation of C-ring diversified andrographolide analogs **4** and **5**. b) Color-coded fluorines on N-phenyl triflate and the triflate ion that refer to similarly highlighted peaks on the following NMR time course c) <sup>19</sup>F NMR time course showing the disappearance of N-phenyl triflate (-71.6 ppm) and appearance of triflate anion (-79.3 ppm). The absence of C14-triflated andrographolide on the NMR time course suggests that initial triflation is rate determining over elimination of the 14- $\alpha$ -triflate adduct.

separable and distinguishable by NMR given the change in splitting patterns occurring in each diene system.

### Michael Addition Assay

In order to quantitatively measure the efficacy of the Michael acceptor properties of each compound, we monitored the reaction between a free thiol source (glutathione) with each compound, utilizing 5,5'-dithiobis(2-nitrobenzoic acid) (DTNB; "Elleman's reagent") for the colorimetric quantification of free thiols in solution (31). Free thiols cleave the disulfide bond in colorless DTNB, which then ionizes into the bright yellow TNB<sup>2-</sup> dianion with a maximal absorbance at 410 nm (32). This method is advantageous since the reaction is rapid and stoichiometric; one mole of DTNB will release exactly one mole of TNB<sup>2-</sup> in presence of a free thiol nucleophile (33). We used a standard curve of glutathione concentration compared to DTNB conversion to determine the relationship between absorbance and concentration of TNB<sup>2-</sup>. We then derived the relative Michael addition kinetics of andrographolide and our synthesized analogs from the absorbance. Using a plate reader set to measure the absorbance at 410 nm, we conducted high-throughput screening of our compounds. Liquid chromatography-mass spectrometry confirmed the formation of the dehydrated form of the andrographolide-glutathione adduct at the observed molecular weight of 638.51 m/z (expected 638.274 m/z).

Consistent with our initial expectations, andrographolide (Compound 1) and acetone (Compound 2) performed equally well as Michael acceptors. Compound 4 demonstrated similar Michael acceptor abilities as andrographolide, indicating that the elimination of the hydroxyl group at C14 does not affect Michael acceptor capabilities. However, compound 5 proved to be a significantly better Michael acceptor in comparison to compound 1, as supported by the faster decrease in glutathione concentration and absorbance at 410 nm. Contrary to initial expectations, compound 3, with an acetate in place of a hydroxyl at C-14, demonstrated the poorest Michael acceptor kinetics compared to the other analogs (Figure 4).

### Computational Modeling

To investigate whether trends observed in the *ex vivo* Michael addition assay were a function of electronics or sterics, we performed computational studies to model the Michael addition energetic pathways of andrographolide and each analog. We found the single point energies (SPE), or the potential energy of a molecule for a specific arrangement of atoms, of each compound at each intermediate, using N-acetyl-L-cysteine as the surrogate Michael donor, and identified the relative differences in energy between each intermediate. The energetic pathways for all analogs were relatively consistent, suggesting that changes in sterics may play a more significant role in defining Michael addition kinetics (Figure 5).

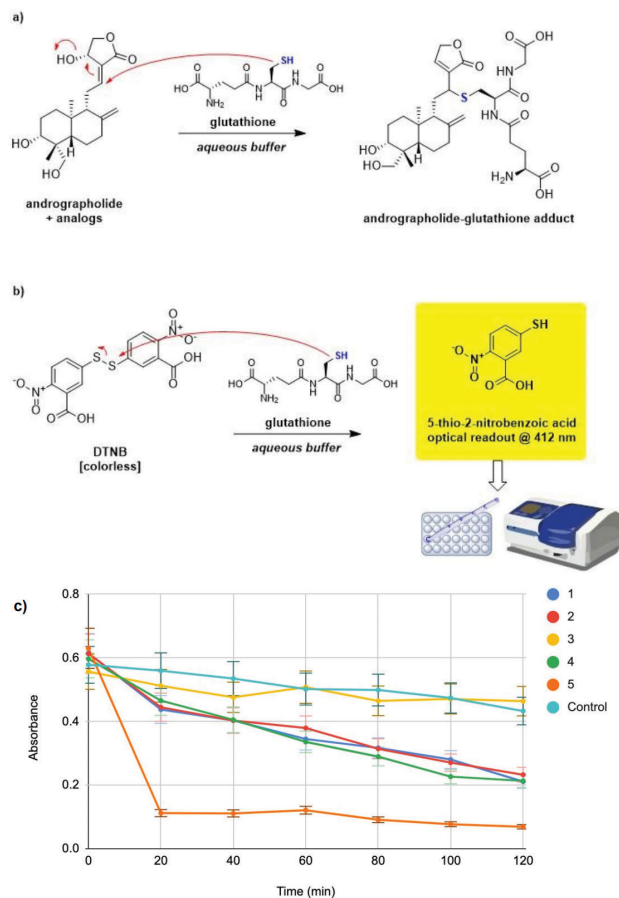


**Figure 4: *Ex vivo* reactivity assay performed on andrographolide and synthetic analogs provides insight into structure-reactivity relationship.** a) The mechanism of action of the thiol-Michael Addition between andrographolide and glutathione in an aqueous buffer to produce the andrographolide-glutathione adduct. b) Free thiols in aqueous solution cleave the disulfide bond in colorless DTNB, which then ionizes to the yellow TNB<sup>2-</sup> dianion. c) Michael Addition Assay data which shows reduced glutathione (GSH) consumption by the andrographolide related compounds over time. The y-axis represents absorbance of the well at 420 nm. With the assays run in triplicate, the error bars represent the standard error at every time interval. The control (assays performed that incubated GSH without an andrographolide or an andrographolide analog) establishes that GSH auto-oxidizes to oxigluthathione (GSSG) at a negligible rate. All experiments were performed in triplicate.

### DISCUSSION

In this study, both 14-deoxy-11,12-didehydroandrographolide (Compound 5) and 14-deoxy-14,15-didehydro andrographolide (Compound 4) were semi-synthesized via the subjection of 3,19-isopropylidene andrographolide to N-phenyl triflate and DBU in an efficient one-pot synthesis exhibiting full conversion within minutes. The two products were synthesized through E2 and E2' mechanisms. Neither mechanism seemed to be favored with these conditions. N-phenyl triflate was used because the reaction could be conveniently monitored via <sup>19</sup>F NMR, as the waning fluorine peak was inversely proportional to reaction progress as the triflate group was eliminated through

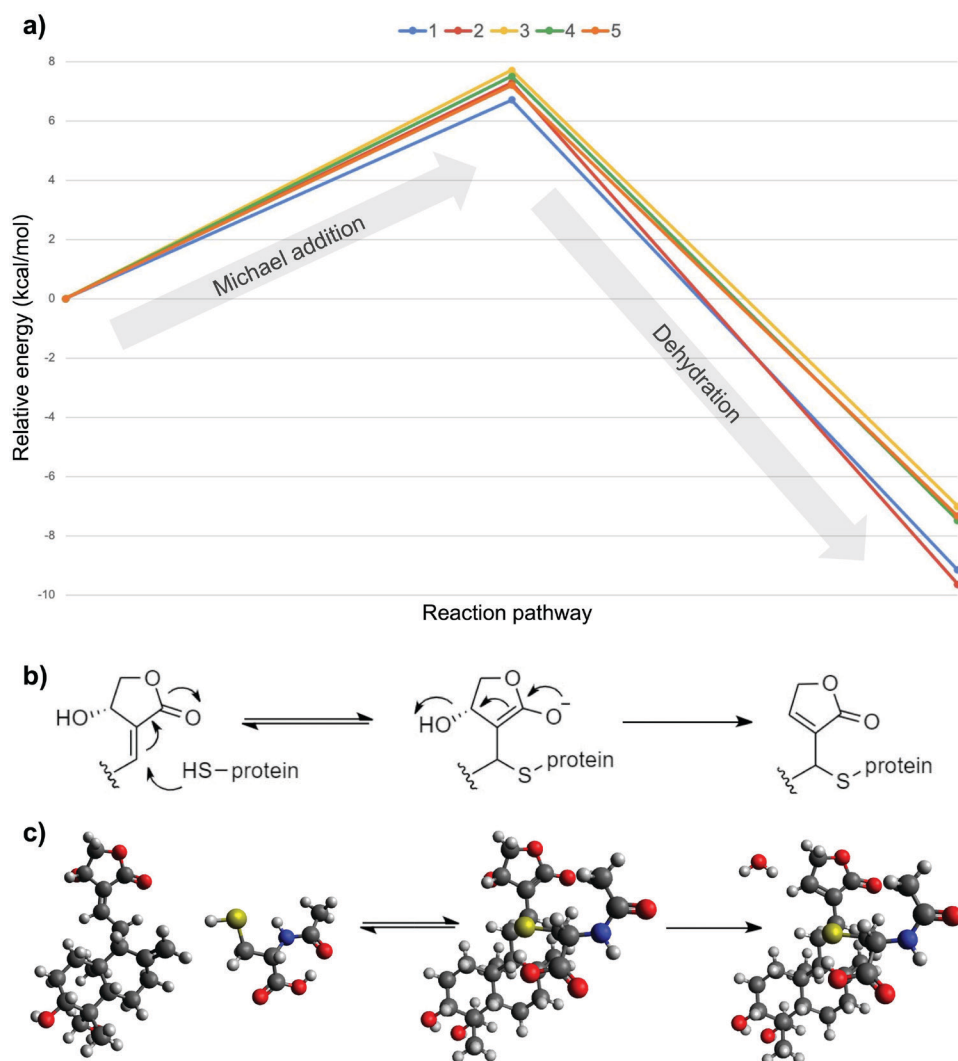


**Figure 5: In silico modeling of the energetic favorability of Michael addition by andrographolide and four analogs.** a) The relative energetic pathway of each compound along Michael addition and subsequent dehydration. b) The mechanism of action through which andrographolide forms a covalent adduct on cysteine residues of proteins, comprising Michael addition and irreversible dehydration. c) Computational model generated on Avogadro that depicts the mechanism through which andrographolide forms a covalent adduct on N-acetyl-L-cysteine.

both mechanisms.  $^{19}\text{F}$  NMR provides a more informative mode of reaction tracking than Thin Layer Chromatography (TLC), as it allows for quantitative reaction tracking via kinetics experiments (34). However, it was also discovered that 14-deoxy-11,12-didehydroandrographolide could be synthesized via the subsection of 3,19-isopropylidene andrographolide to DBU only, exhibiting full conversion after stirring overnight. We have concluded that the incorporation of N-phenyl triflate in the reaction mixture allows for full conversion within a significantly shorter timeframe. Further mechanistic studies to elucidate the formation of 14-deoxy-11,12-didehydroandrographolide are underway.

We used  $^1\text{H}$  NMR to characterize both products of this reaction. A retained C-14 proton, which existed as a doublet, and the addition of a singlet corresponding to the acetate around 2 ppm helped identify compound **3**. Additionally, the

C-14 alcohol was absent in the spectra, and the C-15 protons were observed far downfield, as expected in the  $^1\text{H}$  NMR of compound **3**. The C-11 proton, which existed as a doublet of doublets, with one J-value corresponding to a *trans* alkene, helped characterize compound **5**. Further, we extrapolated the C-12 and C-10 protons from COSY cross peaks, and the C-14 on this compound was expressed as a singlet on the  $^1\text{H}$  NMR spectra of compound **5**, which is expected due to lack of coupling between C-14 and C-15. For more detailed spectral data, please refer to pages 7-10 and 16-19 of the Supporting Information document.

Through *ex vivo* screening, we developed an efficient, high-throughput method for the screening of Michael addition onto DTNB while also evaluating the Michael accepting abilities of our studied compounds. Since the olefin at C-17 may obstruct the ability of proteins such as glutathione to

access the Michael donor at C-12, we hypothesized that the enhanced reactivity of compound **5** is due to a reduction of steric hindrance resulting from the migration of the Michael acceptor from C-12 to C-14. Moreover, although we predicted that the more favorable acetate leaving group at C-14 would accelerate Michael addition kinetics, our *ex vivo* experimental results supported the opposite results, which we predict is due to changes in the conformation of compound **3** that impede access to the C-12 Michael donor.

Further computational investigations confirmed that relative differences in Michael accepting abilities are more influenced by steric rather than electronic factors. The energetic topography for the Michael addition of each analog was constructed and suggested that all compounds followed a relatively uniform energetic pathway. Interestingly, compound **1** exhibited the lowest energetic threshold for initial Michael addition, with **2** and **5** following a mechanism less favorable by 0.5 kcal/mol. Consistent with experimental results, **3** followed a pathway with the greatest energetic barrier, incurring thermodynamic penalties that support reduced Michael addition abilities *ex vivo*. These computational experiments support the observation in the Michael addition colorimetric assay that the addition kinetics are largely a function of sterics and provide insight into strategies that may improve the reactivity of andrographolide through stereoelectronic modifications.

Thus, we report the semi-synthesis, NMR characterization, and Michael acceptor efficiencies of four andrographolide analogs *ex vivo* and *in silico*; two of these studied analogs are conveniently accessed through a triflation-elimination reaction that can be tracked by  $^{19}\text{F}$  NMR spectroscopy. We identified that migration of the Michael acceptor position from C-12 to C-14 greatly increases the rate of Michael addition when treated with a free thiol such as glutathione. To further corroborate this finding, we performed computational modeling to identify the roles of steric and electronic effects in causing this difference in reactivity. These results demonstrate new synthetic routes toward the access of such compounds and shed light into chemical modifications that may result in the development of potential clinical agents. *In vitro* studies on the biological activity of these compounds, as well as efforts in further analog syntheses, are currently underway in our laboratory.

## MATERIALS AND METHODS

### Synthesis of Andrographolide-3,19-acetonide (**2**)

We synthesized acetonide (Compound **2**) from andrographolide (Compound **1**) by reaction with 2,2-dimethoxypropane (20 mL, 4.38 mmol, 4.3 eq.) and catalytic pyridinium p-toluenesulfonate (PPTS) (441 mg, 5.5 mmol, 5.5 eq.) in anhydrous acetone (20 mL). We monitored the reaction by thin layer chromatography (TLC, 1:1 ethyl acetate / hexanes as an eluent) and observed complete conversion of the starting material after 30 minutes. The reaction mixture was filtered through a plug of sodium

carbonate and concentrated in a rotary evaporator, and the product, acetonide (Compound **2**), was purified by silica gel flash chromatography.

### Synthesis of 14-acetylandrographolide Acetonide (**3**)

To install the C14 acetate, we followed literature conditions of adding one gram of acetonide (Compound **2**) in neat acetic anhydride (4.3 mL, 45.5 mmol, 20 eq) and heating it on a heating stir plate for two hours (29). This reaction mixture was cooled and directly loaded onto a silica gel flash column to purify acetate compound **3** as an off-white gel in approximately 75% yield.

### Synthesis of 14,15-didehydro-14-deoxyandrographolide Acetonide (**4**)

To synthesize elimination product **4**, we dissolved acetonide **2** (680 mg, 1.74 mmol, 1 eq.) in methylene chloride (5.2 mL) and sequentially added acetic anhydride (980  $\mu\text{L}$ , 10.4 mmol, 6 eq.), triethylamine (1.00 mL, 7.8 mmol, 4.5 eq.) and DMAP (288 mg, 2.36 mmol, 1.35 eq.). The reaction was stirred for fifteen minutes upon which full conversion of starting material was observed by thin layer chromatography. The reaction material was directly flushed through flash chromatography whereby an eluent of 25% ethyl acetate in hexanes afforded alkene **4** (590 mg, 81% yield) as a white solid. Alternatively, we found that treatment of 14-acetylandrographolide acetonide (Compound **3**) with triethylamine also afforded compound **4**.

### Synthesis of 11,12-didehydro-14-deoxyandrographolide acetonide (**5**)

To synthesize elimination product **5**, we added andrographolide acetonide (Compound **2**) (250 mg, 0.64 mmol, 1.0 eq) in acetonitrile (mL, HPLC grade) to a 50 mL round bottom flask with a Teflon stir bar. To this solution, 1,8-Diazabicyclo[5.4.0]undec-7-ene (DBU, 0.382 mL, 2.6 mmol, 4 eq) was added dropwise, followed by N-phenyl triflate (PhNTf<sub>2</sub>, 459 mg, 1.3 mmol, 2 eq.) was added as a single portion. The reaction was stirred for 10 minutes, and we monitored reaction progress by thin layer chromatography (TLC, UV/PMA stain) and by  $^{19}\text{F}$  nuclear magnetic resonance (NMR) spectroscopy. The starting material was determined to have fully converted by TLC after 20 minutes, and this was verified to be the desired elimination product by the appearance of stoichiometric formation of the triflate anion ( $^{19}\text{F}$   $\delta$  = -79.254 ppm in CH<sub>3</sub>CN). The reaction was quenched by the addition of an aqueous solution of ammonium chloride (100 mL, 0.1 M) and extracted in two portions of methylene chloride. The resulting organic layers were dried over anhydrous magnesium sulfate and concentrated *in vacuo* with a rotary evaporator, and then purified on silica gel flash chromatography using a gradient of 100% hexane to 60% hexane in ethyl acetate to afford compound **4** (41 mg, 17 % yield) and compound **5** (62 mg, 26 % yield) as yellow oils.

	Compound 2	Compound 3	Compound 4	Compound 5
C-11	$\delta = 2.47$ , 2H, m, $J = 2.47$ Hz	$\delta = 2.41$ , 2H, dd, $J = 6.6$ Hz	$\delta = 6.91$ , 1H, dd, $J = 16.29$	$\delta = 7.11$ , 1H, dd, $J = 15.8\text{Hz}, 10\text{Hz}$
C-12	$\delta = 6.60$ , 1H, t, $J = 6.83$ Hz	$\delta = 7.01$ , 1H, t, $J = 6.7$ Hz	$\delta = 6.11$ , 1H, d, $J = 15.81$ Hz	$\delta = 6.41$ , 1H, d, $J = 15.8\text{Hz}$
C-14	$\delta = 4.92$ , 1H, m, $J = 6.03$ Hz	$\delta = 5.93$ , 1H, d, $J = 5.9$ Hz	$\delta = 6.21$ , 1H, dd, $J = 0.8, 3.5$ Hz	$\delta = 7.34$ , 1H, s
C-15	(a) $\delta = 4.37$ , 1H, m, $J = 5.99, 9.90$ Hz (b) $\delta = 4.01$ , 1H, dd, $J = 1.89, 9.96$ Hz	(a) $\delta = 4.90$ , 1H, m (b) $\delta = 4.30$ , 1H, dd, $J = 6.4$ Hz	$\delta = 6.81$ , 1H, d, $J = 3.6$	$\delta = 4.99$ , 2H, s

**Table 1:** Chemical shift ( $\delta$ ), proton count, splitting pattern, and J-value (Hz) of diagnostic peaks C-11, C-12, C-14, and C-15 determined through  $^1\text{H}$  NMR spectroscopy. On low field NMR spectra, peak assignments and coupling constants were extracted from correlation spectroscopy (COSY) and J-resolved (JRES) spectra.

### Reagents

Chemical reagents used include andrographolide (95%, AK Scientific), 2,2-dimethoxypropane (98%, AK Scientific), pyridine (98%, Beantown Chemical), p-toluenesulfonic acid (98%, monohydrate, GFS Chemicals), acetone (Acros Organics), Dess-Martin Periodinane (95%, AK Scientific), N-phenyl triflate (95%, AK Scientific), DBU (95%, AK Scientific), and acetonitrile (HPLC grade, Carolina Chemical). All reagents were used without further purification. Solvents used in purification were purchased from Stellar Chemical, JT Baker, or Fisher and used without further purification.

### Characterization

All compounds were characterized by  $^1\text{H}$  and  $^{13}\text{C}$  NMR via a Nanalysis NMReady 60 MHz nuclear magnetic resonance spectrometer in deuterated chloroform (99.98% D, with 1% v/v tetramethylsilane (TMS) as an internal standard) and Fourier-transform infrared (FT-IR) spectroscopy (Thermo Scientific iS5 Nicolet FT-IR spectrometer, iD5 ATR assembly). The structures of compounds **3**, **4**, and **5** were assigned on the basis of diagnostic peaks of the C-ring and were found to be in complete agreement with literature values (**Table 1**). Full characterization and spectroscopic data are available in the Supplementary Information document.

### Michael Addition Assays

We prepared a 10 mM DTNB stock solution by adding 40 mg of DTNB to 10 mL of DMSO. To prepare a 5 mM working solution of DTNB, we added 1 mL DTNB stock solution to 1 mL DMSO. We prepared a buffer solution of 75% HEPES buffer and 25% DMSO by adding 45 mL of 20 mM HEPES buffer at pH 6.5 in deionized water to 15 mL of DMSO. Immediately before starting the assay, we prepared a fresh 5 mM solution of GSH by adding reduced-glutathione to the HEPES-DMSO buffer. Then, we added 1 mL of the reduced glutathione (GSH) solution along with enough andrographolide/andrographolide analog to make a

5 mM solution of the compound. We incubated the solution at 37 °C for the duration of the assay. We performed the colorimetric analysis on a 96-well plate, and absorbance was measured using a plate reader at 412 nm. On the 96-well plate, we established a control by filling three wells with 30  $\mu\text{L}$  DTNB solution and 30  $\mu\text{L}$  HEPES-DMSO buffer at pH 6.5. We took triplicate samples of each of the three incubated reaction mixtures by adding 30  $\mu\text{L}$  DTNB solution to 30  $\mu\text{L}$  reaction mixture in each well. We measured each sample every 20 minutes starting from 0 minutes to 120 minutes, and absorbance was taken 15 minutes after each set of samples were taken to allow for DTNB to react. Absorbance was recorded as an average of each set of triplicates, and this method was repeated for each analog.

### Computational Modeling

Each intermediate involved in the Michael addition reaction for andrographolide and its analogs was constructed virtually on Avogadro and quantum mechanically optimized using density functional theory (DFT) on ORCA, an open source, *ab initio* quantum chemistry molecular modeling software package (35). Subsequently, single point energy (SPE) calculations were performed on DFT-optimized structures and used to construct reaction energetic topographies. Computational simulations and DFT calculations were performed on a Dell Poweredge 710 server with a 24 core Intel Xeon X5660 processor @ 2.80GHz and 32GB RAM. In all DFT calculations, conductor-like polarizable continuum model (CPCM) with the dielectric constant of water was used as the solvation model, B3LYP was used as the basis set, and 6-31G was used as the functional (36).

### ACKNOWLEDGMENTS

We would like to thank the Aspiring Scholars Directed Research program for providing us with lab space as well as the opportunity to conduct high-quality research. We would also like to thank the lab technicians for ensuring our

safety and helping us resolve technical issues while in the laboratory. Last but not least, we gratefully acknowledge the Olive Children Foundation and its community of corporate sponsors and supporters for funding our research.

**Received:** December 18, 2021

**Accepted:** August 23, 2022

**Published:** November 17, 2022

## REFERENCES

1. Vetvicka, Vaclav., and Luca Vannucci, L. "Biological properties of andrographolide, an active ingredient of *Andrographis paniculata*: a narrative review." *Annals of Translational Medicine*, vol. 9, no. 14, Jul. 2021, doi: 10.21037/atm-20-7830.
2. Islam, M., et al. "Andrographolide, a diterpene lactone from *Andrographis paniculata* and its therapeutic promises in cancer." *Cancer Letters*, vol. 420, Feb. 2018, doi: 10.1016/j.canlet.2018.01.074
3. Soo, H. L., et al. "Advances and challenges in developing andrographolide and its analogues as cancer therapeutic agents." *Drug Discovery Today*, vol. 24, no. 9, Sept. 2014, doi: 10.1016/j.drudis.2019.05.017.
4. Mishra, A., et al. "Andrographolide: A Herbal-Chemosynthetic Approach for Enhancing Immunity, Combating Viral Infections, and Its Implication on Human Health." *Molecules*, vol. 26, no. 22, Nov. 2021, doi: 10.3390/molecules26227036.
5. Tran, Q. T. N., et al. "Polypharmacology of andrographolide: beyond one molecule one target." *Natural Product Reports*, vol. 38, iss. 4, Apr. 2021. doi: 10.1039/d0np00049c.
6. Handa, S.S. and Sharma, A. "Hepatoprotective activity of andrographolide from *Andrographis paniculata* against carbon tetrachloride." *The Indian J. of Med. Res.*, vol. 92, pp. 276, Aug. 1990
7. Jayakumar, T., et al. "Experimental and Clinical Pharmacology of *Andrographis paniculata* and Its Major Bioactive Phytoconstituent Andrographolide." *Evidence-Based Complementary and Alternative Medicine*, vol. 2013, Mar. 2013, doi: 10.1155/2013/846740.
8. Rajagopal, S., et al. "Andrographolide, a potential cancer therapeutic agent isolated from *Andrographis paniculata*." *Journal of Exp. Ther. and Onc.*, vol. 3, no. 3, pp.147-158, May 2003, doi: 10.1046/j.1359-4117.2003.01090.x.
9. Kumar, G., et al. (2020) "Andrographolide: Chemical modification and its effect on biological activities." *Bioorganic Chemistry*, vol. 95, Dec. 2020, doi: 10.1016/j.bioorg.2019.103511.
10. Soo, H. L., et al. "Advances and challenges in developing andrographolide and its analogues as cancer therapeutic agents." *Drug Discovery Today*, vol. 24, no. 9, pp.1890-1898, Sept. 2019, doi: 10.1016/j.drudis.2019.05.017.
11. Nguyen, V. S., et al. "Specificity and inhibitory mechanism of andrographolide and its analogues as antiasthma agents on NF- $\kappa$ B p50." *J Nat Prod.*, vol. 78, no. 2, pp.208-17, Jan. 2015, doi: 10.1021/np5007179.
12. Wanandi, S. I., et al. "In silico and in vitro studies on the anti-cancer activity of andrographolide targeting survival in human breast cancer stem cells." *PLOS ONE*, vol. 15, no.11, Nov. 2020, doi: 10.1371/journal.pone.0240020.
13. Liu, B., et al. "Cyclooxygenase-2 promotes tumor growth and suppresses tumor immunity." *Cancer Cell Int*, vol. 15, no. 106, Nov. 2015, doi: 10.1186/s12935-015-0260-7.
14. Kajal, K., et al. "Andrographolide binds to ATP-binding pocket of VEGFR2 to impede VEGFA-mediated tumor-angiogenesis." *Sci Rep*, vol. 9, Mar. 2019, doi: 10.1038/s41598-019-40626-2.
15. Reabroi, S., et al. "The anti-cancer activity of an andrographolide analogue functions through a GSK-3 $\beta$ -independent Wnt/ $\beta$ -catenin signaling pathway in colorectal cancer cells." *Sci Rep*, vol. 8, no. 7924, May 2018, doi: 10.1038/s41598-018-26278-8
16. Das, B. et al. "Synthesis, cytotoxicity, and structure-activity relationship (SAR) studies of andrographolide analogues as anti-cancer agent." *Bioorg. Med. Chem. Lett*, vol. 20, pp. 6947–6950, Dec. 2010, doi: 10.1016/j.bmcl.2010.09.126.
17. Gersch, M., et al. "Electrophilic natural products and their biological targets." *Nat Prod Rep.*, vol. 29, pp.:659–682. June 2012. doi: 10.1039/c2np20012k.
18. Xia, Y. F. et al. "Andrographolide Attenuates Inflammation by Inhibition of NF- $\kappa$ B Activation through Covalent Modification of Reduced Cysteine 62 of p50." *J Immunol*, vol. 173 no. 6, pp.4207-4217, Sept. 2004, doi:10.4049/jimmunol.173.6.4207.
19. Nie, X., et al. "Attenuation of Innate Immunity by Andrographolide Derivatives Through NF- $\kappa$ B Signaling Pathway." *Sci. Rep.*, vol. 7, no. 4738, Jul. 2017, doi: 10.1038/s41598-017-04673-x.
20. Ciampi, E., et al. "Efficacy of andrographolide in not active progressive multiple sclerosis: a prospective exploratory double-blind, parallel-group, randomized, placebo-controlled trial." *BMC Neurology*, vol. 20, no. 173, May 2020, doi: 10.1186/s12883-020-01745-w.
21. Calabrese, C., et al. "A phase I trial of andrographolide in HIV positive patients and normal volunteers." *Phyt. Res.*, vol. 14, no. 5, pp.333-338. Aug. 2000, doi: 10.1002/1099-1573(200008)14:5<333::aid-ptr584>3.0.co;2-d.
22. Aromdee, C. "Modifications of andrographolide to increase some biological activities: a patent review (2006 – 2011)." *Expert Opinion on Therapeutic Patents*, vol. 22, no. 2, pp.169-180, Feb. 2012, doi: 10.1517/13543776.2012.661718.
23. Rajani, M., et al. "A rapid method for isolation of andrographolide from *andrographis paniculata* nees (kalmegh)." *Pharm Biol*, vol. 38, no. 3, pp.204-209. Jan 2011, doi: 10.1076/1388-0209(200007)3831-SFT204
24. Newman, D. J., et al. "The influence of natural products

- upon drug discovery." *Natural Product Reports*, vol. 17, no. 3, pp.215-234, Jun. 2000, doi: 10.1039/a902202c.
25. Newman, D. J., and Cragg, G. M. "Natural products as sources of new drugs over the nearly four decades from 01/1981 to 09/2019." *Journal of Natural Products*, vol. 83, no. 3, pp.770-803, Mar. 2020, doi: 10.1021/acs.jnatprod.9b01285.
26. Majhi, S., and Das, D. "Chemical derivatization of natural products: Semisynthesis and pharmacological aspects-A decade update." *Tetrahedron*, 78:131801. 2020 doi: 10.1016/j.tet.2020.131801
27. Oh, E.T., *et al.* "Docetaxel induced-JNK2/PHD1 signaling pathway increases degradation of HIF-1 $\alpha$  and causes cancer cell death under hypoxia." *Sci. Rep.*, vol. 6, no. 27382. June 2016, doi: 10.1038/srep27382.
28. Lim, J.C.W., *et al.* "Andrographolide and its analogues: versatile bioactive molecules for combating inflammation and cancer." *Clinical and Experimental Pharmacology and Physiology*, vol. 39, pp. 300-310, Mar. 2012, doi: 10.1111/j.1440-1681.2011.05633.x.
29. Xin, Z., *et al.* "Stereoselective Synthesis and Biological Evaluation of ent -Asperolide C and its Analogues." *European Journal of Organic Chemistry*, vol. 2018, no. 4, pp.477-484, Dec. 2017, doi: 10.1002/ejoc.201701292.
30. Tran, Q. T., *et al.* "From irreversible to reversible covalent inhibitors: Harnessing the andrographolide scaffold for anti-inflammatory action." *European Journal of Medicinal Chemistry*, vol. 204, no. 112481. Oct. 2020, doi: 10.1016/j.ejmech.2020.112481
31. Riener, C. K., *et al.* "Quick measurement of protein sulfhydryls with Ellman's reagent and with 4,4'-dithiodipyridine." *Anal Bioanal Chem*, vol. 373, no. 4-5, pp. 266-276, Jul. 2002, doi: 10.1007/s00216-002-1347-2.
32. Walmsley, T. A., *et al.* "Effect of daylight on the reaction of thiols with Ellman's reagent, 5,5'-dithiobis(2-nitrobenzoic acid)." *Clin Chem*, vol. 33, no. 10, pp.1928-31, Oct. 1987.
33. Winther, J. R., and Thorpe, C. "Quantification of thiols and disulfides." *Biochimica et Biophysica Acta*, vol. 1840, no. 2, pp. 838-846, Feb. 2014, doi:10.1016/j.bbagen.2013.03.031
34. Do, N. M., *et al.* "Application of Quantitative  $^{19}\text{F}$  and  $^1\text{H}$  NMR for Reaction Monitoring and In Situ Yield Determinations for an Early Stage Pharmaceutical Candidate." *Anal. Chem*, vol. 83, no. 22, pp.8766-8771, Oct. 2011, doi: 10.1021/ac202287y
35. Neese, Frank, *et al.* "The ORCA program system." *Wiley Interdisciplinary Reviews: Computational Molecular Science*, vol. 2, no. 1, pp. 73-78, Jun. 2011, doi: 10.1002/wcms.81.
36. Takano, Yu, *et al.* "Benchmarking the conductor-like polarizable continuum model (CPCM) for aqueous solvation free energies of neutral and ionic organic molecules." *Journal of Chemical Theory and Computation*, vol. 1, no. 1, pp. 70-77, Jan. 2005, doi:

10.1021/ct049977a.

**Copyright:** © 2022 Zhou, Chang, Wang, Wu, Kocalar, Swaminathan, Rao, Athreya, Chanda, and Njoo. All JEI articles are distributed under the attribution non-commercial, no derivative license (<http://creativecommons.org/licenses/by-nc-nd/3.0/>). This means that anyone is free to share, copy and distribute an unaltered article for non-commercial purposes provided the original author and source is credited.

# Supporting Information for ***Reactivity-informed design, synthesis, and Michael addition kinetics of C-ring andrographolide analogs***

Alice Zhou, Warren Chang, Tiffany Wang, Jeslyn Wu, Selin Kocalar, Lakshman Swaminathan, Aishi Rao, Priya Chanda, Edward Njoo

Department of Chemistry, Biochemistry & Physics,  
Aspiring Scholars Directed Research Program, Fremont, California

*Correspondence: edward.njoo@asdrp.org*

1. General Information	2
2. Spectroscopic data and experimental procedures	
a. Compound 2 (andrographolide acetonide)	3-6
b. Compound 3 (andrographolide acetate)	7-10
c. Compound 4 (14, 15) elimination product	11-15
d. Compound 5 (11, 12) elimination product	16-19
3. <i>In silico</i> modeling	
a. Compound 1	20-21
b. Compound 2	22-23
c. Compound 3	24-25
d. Compound 4	26-27
e. Compound 5	28-29

## 1. General Information

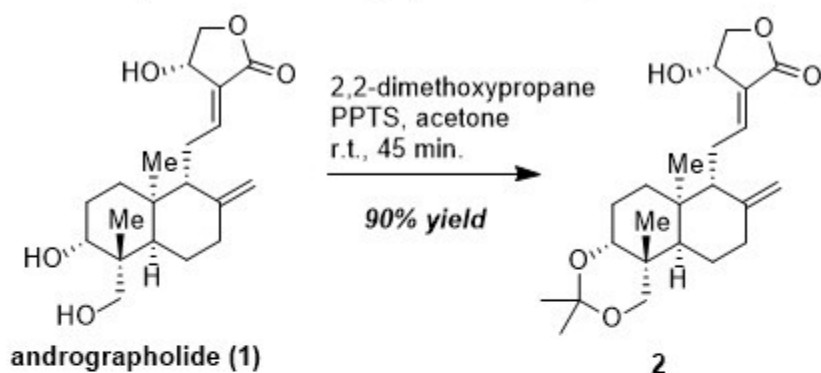
**Materials:** Solvents used in all reactions and purification processes were ACS grade or higher and were used without additional purification, and were purchased from Fisher Chemical, Sigma Aldrich, Sierra Chemical Corp, Beantown Chemical, Stellar Chemical, JT Baker, or Acros Organics. Deuterated solvents were purchased from Cambridge Isotope Laboratories, Acros Organics, or Martek Isotopes, and were used without further purification. All other reagents, catalysts, and chemicals were purchased from commercial sources and used without further purification unless otherwise stated. Solvents used in analytical methods (HPLC, LCMS) were HPLC grade (22 micron filtered).

**Physical methods:**  $^1\text{H}$ ,  $^{19}\text{F}$  and  $^{13}\text{C}\{^1\text{H}\}$  NMR spectra were acquired on a Nanalysis NMReady 60Pro multinuclear benchtop nuclear magnetic resonance spectrometer and were processed on the MestreNova software package.  $^1\text{H}$  and  $^{13}\text{C}\{^1\text{H}\}$  chemical shifts are reported in parts per million (ppm) relative to tetramethylsilane (TMS) as an internal standard. Mass spectra were obtained using a Thermo Scientific LTQ-XL linear ion trap mass spectrometer equipped with a Thermo Finnigan Surveyor reverse phase high performance liquid chromatograph (LC-MS). Infrared spectra were collected on a Thermo Scientific Nicolet iS5 fourier transform infrared (FT-IR) spectrometer equipped with a Thermo iD5 attenuated total reflectance (ATR) assembly. Michael addition assays were performed on a Labsystems Multiskan plate reader with a 410 nm filter.

**Computational methods:** Structural optimization was conducted using density functional theory (DFT) on ORCA, an *ab initio* quantum mechanical molecular modeling suite, at the B3LYP/6-31G level of theory using a CPCM implicit solvation model. DFT, TD-DFT, molecular docking, and molecular dynamics calculations were performed on a Dell PowerEdge 710 server cluster with a 4 x 24 core Intel Xeon X5660 processor at 2.80GHz and 128 GB RAM.

## 2. Spectroscopic Data and Experimental Procedures

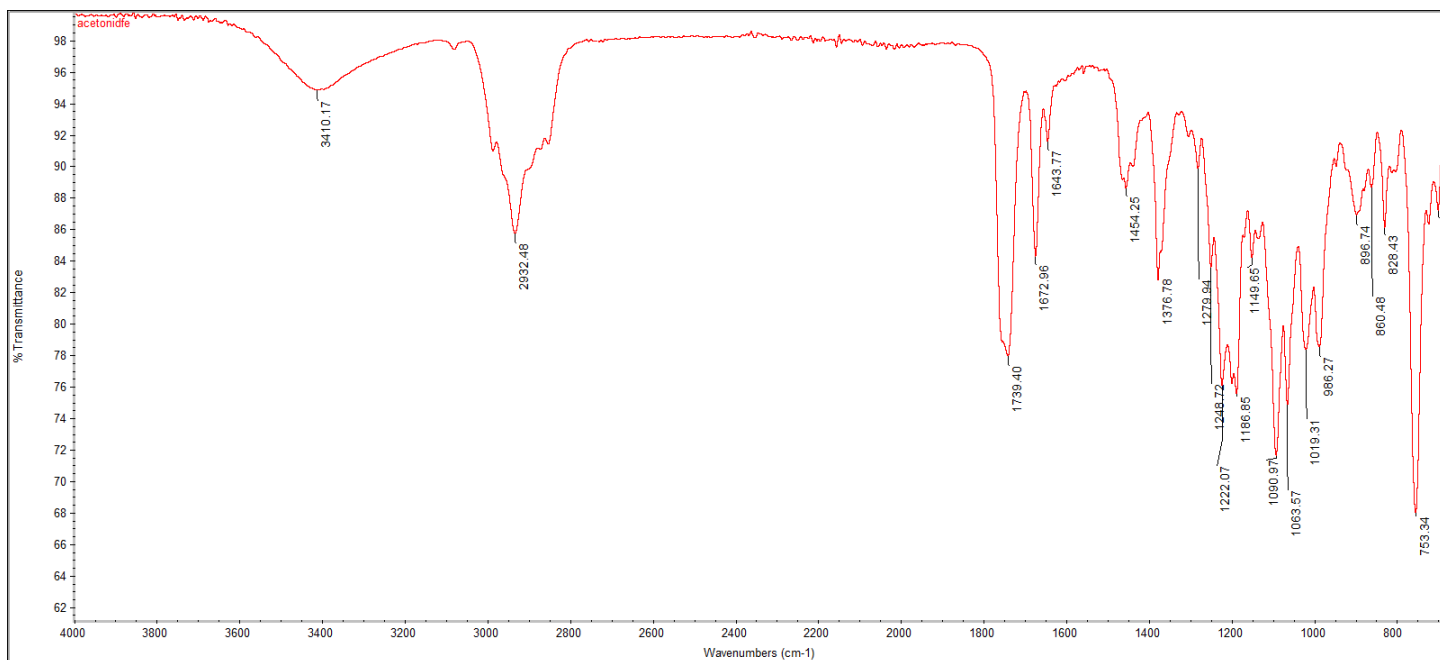
### Compound 2 (andrographolide acetonide)



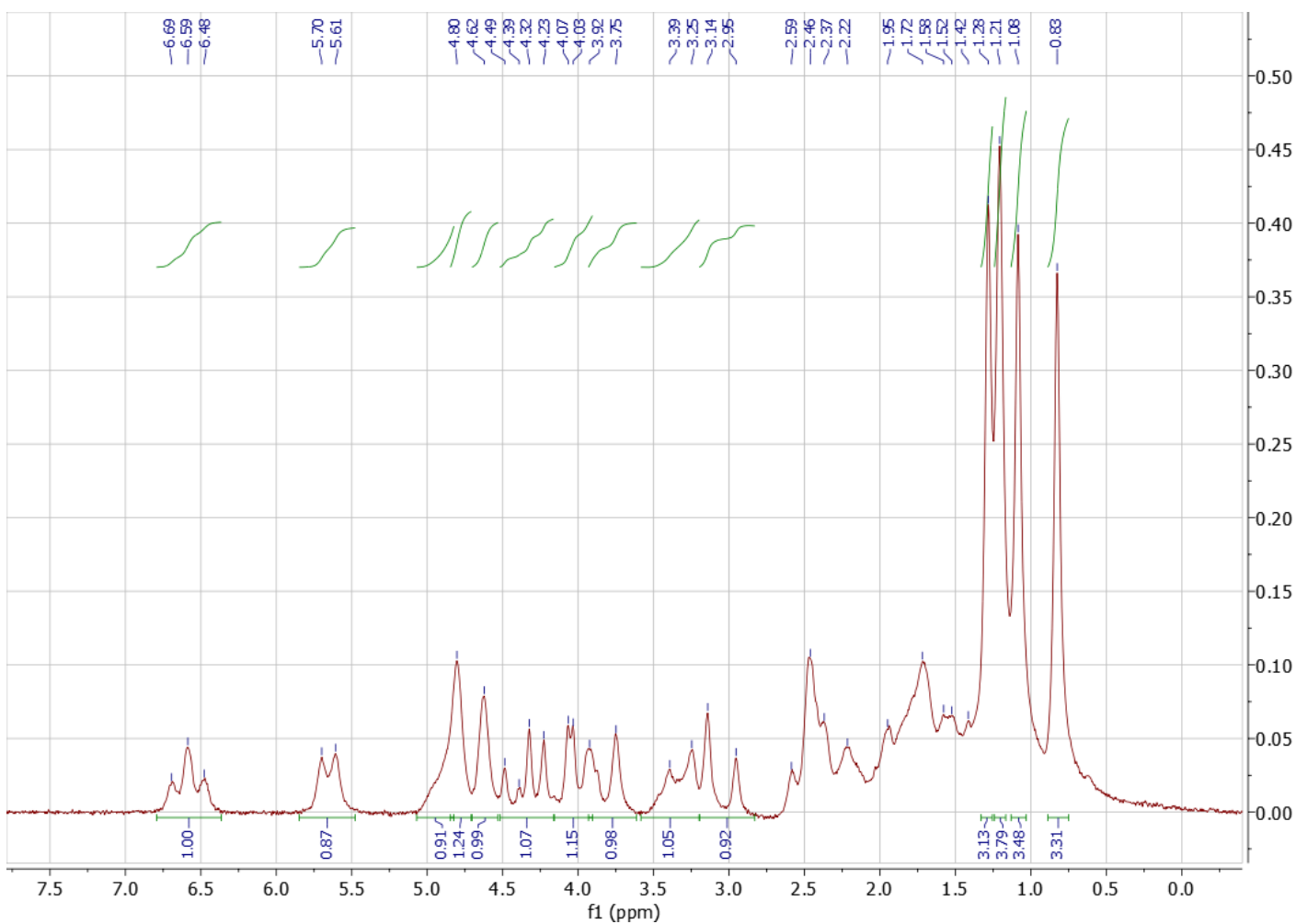
**Experimental procedure:** To a 50 mL round bottom flask charged with a Teflon coated magnetic stir bar was added andrographolide **1** (1.32 g, 1 mmol, 1 eq.) in acetone at a 0.20 M solution. To this, 2,2-dimethoxypropane (20mL, 4.38 mmol, 4.3 eq.) and Pyridinium p-toluenesulfonate (441 mg, 5.5 mmol, 5.5 eq.) was added as a single portion. The reaction mixture was stirred at ambient temperature with a magnetic stir plate, and monitored by thin-layer chromatography (85:15 ethyl acetate in hexanes). Full conversion of the starting material was observed after 30 minutes, upon which the crude reaction was flushed through a plug of anhydrous sodium carbonate and directly concentrated *in vacuo*. The resulting crude material was taken up in DCM, loaded onto a column, and purified via silica gel flash chromatography (10% to 50% ethyl acetate in hexanes, at a 10% gradient) to give the title compound **2** as a white powder in 85% isolated yield.

**Chemicals:** Andrographolide (95%) was purchased from AK Scientific and used without further purification. HPLC grade Acetone was purchased from J.T. Baker. 2,2-dimethoxypropane (95%) and PPTS (95%) was also purchased from AK Scientific and used without further purification. Methylene chloride (ACS grade) was purchased from Stellar Chemical. Silica gel (230-400 mesh) was purchased from Merck, and solvents used in purification were purchased from Alliance Chemicals (ACS grade) and used without further purification.

**TLC**  $R_f$  = 0.45 (50% EtOAc / 50% hexanes), green stain by PMA

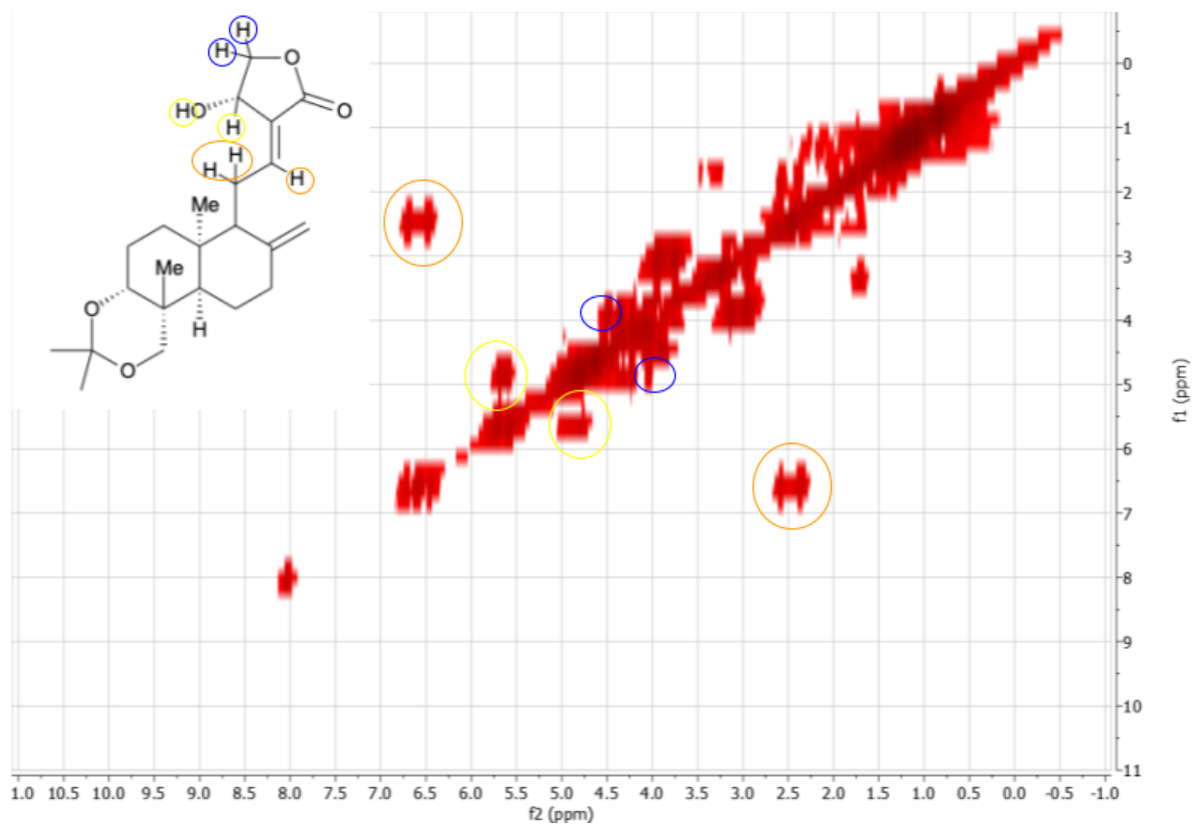


**FT-IR (neat, ATR):** 3410.17, 2932.48, 1739.40, 1672.96, 1643.77, 1454.25, 1376.78, 1279.94, 1248.72, 1222.07, 1186.85, 1149.65, 1090.97, 1063.57, 1019.31, 986.27, 896.74, 860.48, 828.43, 753.34

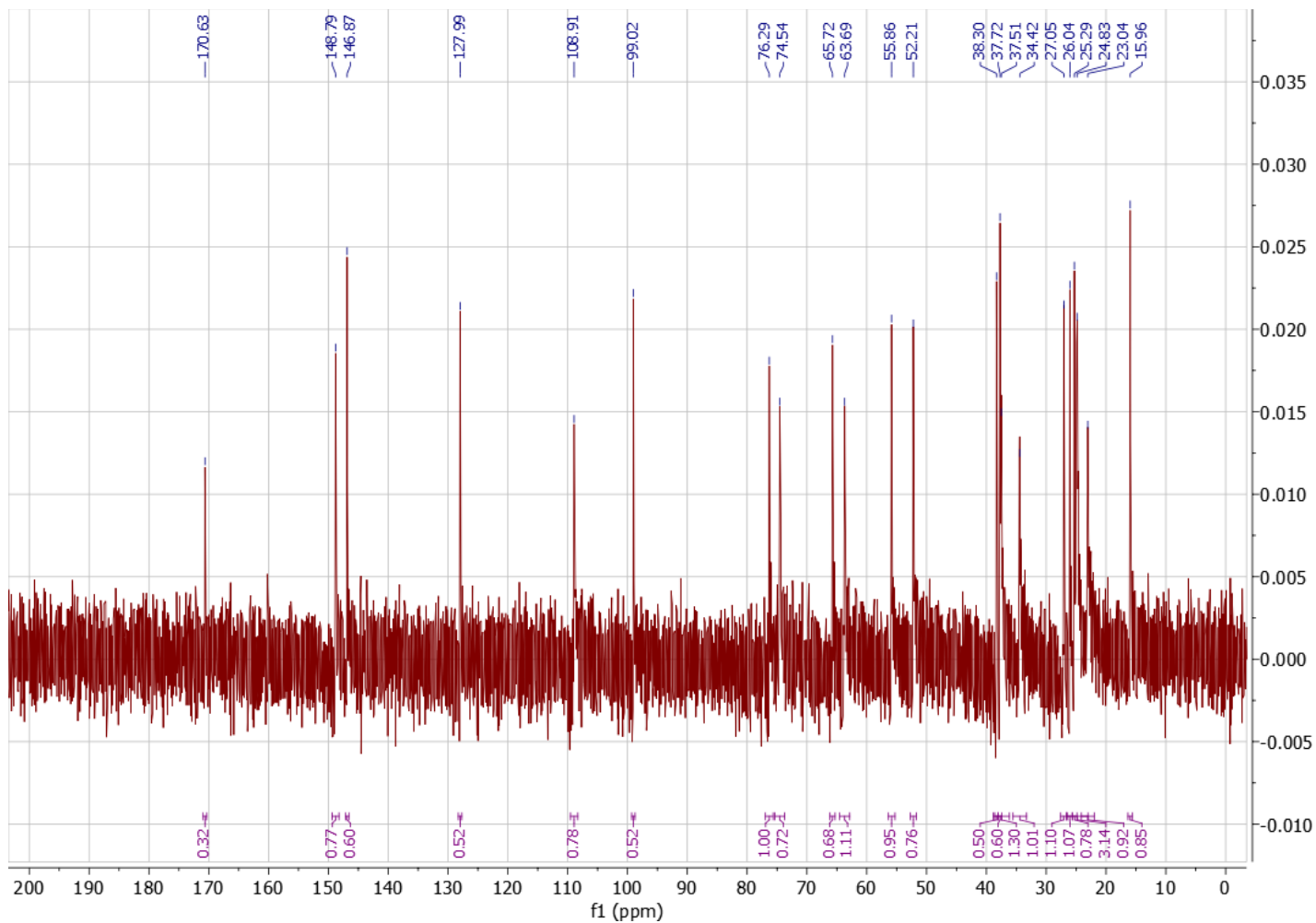


**<sup>1</sup>H NMR** (60 MHz, CDCl<sub>3</sub>) δ, 6.60 (t, J = 6.83 Hz, 1H, C12), 5.66 (d, J = 6.03 Hz, C14 OH), 4.92 (d, J = 6.03 Hz, 1H, C14), 4.82 (s, 1H, C17a), 4.65 (s, 1H, C17b), 4.37 (m, J = 5.99, 9.90 Hz, 1H, C15a), 4.01 (dd, J = 1.89, 9.96 Hz, 1H, C15b), 3.85 (d, J = 11.71 Hz, 1H, C19a), 3.38 (dd, J = 3.09, 9.23 Hz, 1H, C3), 3.08 (d, J = 11.52 Hz, 1H, C19b), 2.47 (m, 2H, C11), 1.57-2.5 (m, J = 3.09, 9.23 Hz, 6H, C2, C5, C7, C9), 1.37 - 1.13 (m, 4H, C1, C6), Acetonide (6H), 0.84 (s, 3H, C20)

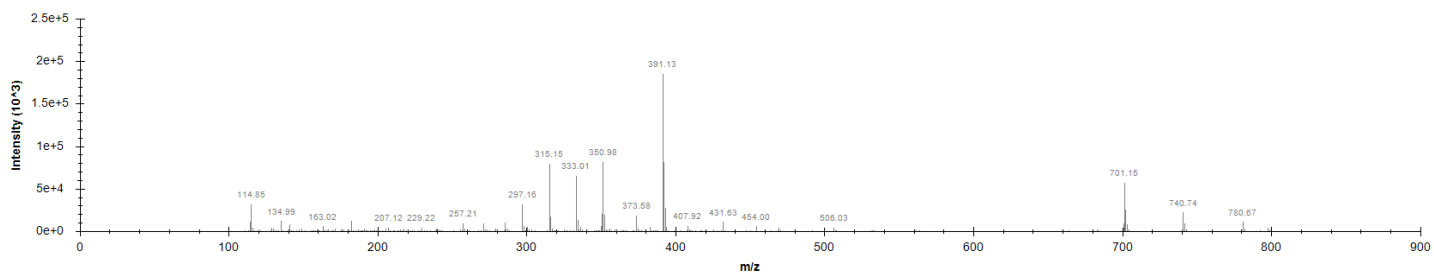
Carbon #	Observed	Literature Reported
C12	6.60 (t, J = 6.83 Hz, 1H)	6.63 (t, J = 6.4 Hz, 1H)
C14 OH	5.66 (d, J = 6.03 Hz)	5.74 (d, J = 6.0 Hz, 1H)
C14	4.92 (d, J = 6.03 Hz, 1H)	4.93 (t, J = 5.8 Hz, 1H)
C17a	4.82 (s, 1H)	4.86 (s, 1H)
C17b	4.65 (s, 1H)	4.69 (s, 1H)
C15a	4.37 (dd, J = 5.99, 9.90 Hz, 1H)	4.41 (dd, J = 6.0, 10.0 Hz, 1H)
C15b	4.01 (dd, J = 1.89, 9.96 Hz, 1H)	4.04 (dd, J = 1.8, 9.8 Hz, 1H)
C19a	3.85 (d, J = 11.71 Hz, 1H)	3.89 (d, J = 11.6 Hz, 1H)
C3	3.38 (dd, J = 3.09, 9.23 Hz, 1H)	3.42 (dd, J = 3.6, 9.2 Hz, 6H)
C19b	3.08 (d, J = 11.52 Hz, 1H)	3.12 (d, J = 11.6, 1H)
C11	2.47 (m, 2H)	2.54–2.50 (m, 1H)
C2, C5, C7, C9	1.57-2.5 (m, J = 3.09, 9.23 Hz, 6H)	2.40– 1.88 (m, 3H) 1.78–1.63 (m, 3H)
C1, C6	1.37 - 1.13 (m, 4H)	1.34 (s, 2H) 1.26 (s, 2H)
Acetonide	(m, 6H)	1.34– 1.15 (m, 3H) 1.14 (s, 3H)
C20	0.84 (s, 3H)	0.88 (s, 3H)



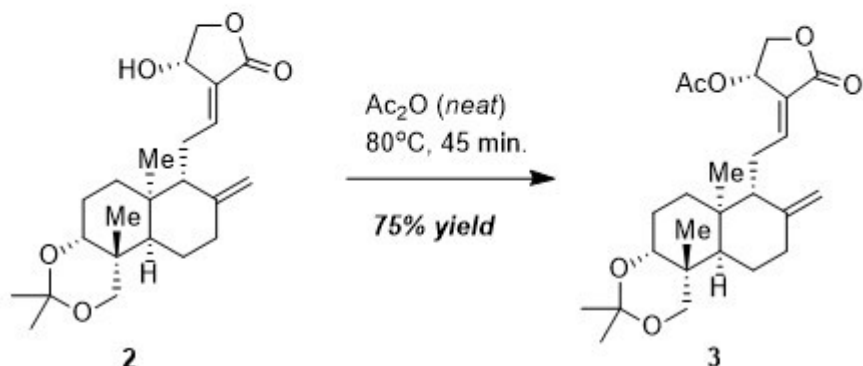
$^1\text{H}$ - $^1\text{H}$  COSY NMR



**13C NMR** (15 MHz, CDCl<sub>3</sub>) δ 170.63, 148.79, 146.87, 127.99, 108.91, 99.02, 76.29, 74.54, 65.72, 63.69, 55.86, 52.21, 38.30, 37.72, 37.51, 34.42, 27.05, 26.04, 25.29, 24.83, 23.04, 15.96.



**ESI-MS** (m/z): [M+H]<sup>+</sup> calc'd for C<sub>23</sub>H<sub>33</sub>O<sub>5</sub>: 389.23, found: 391.13

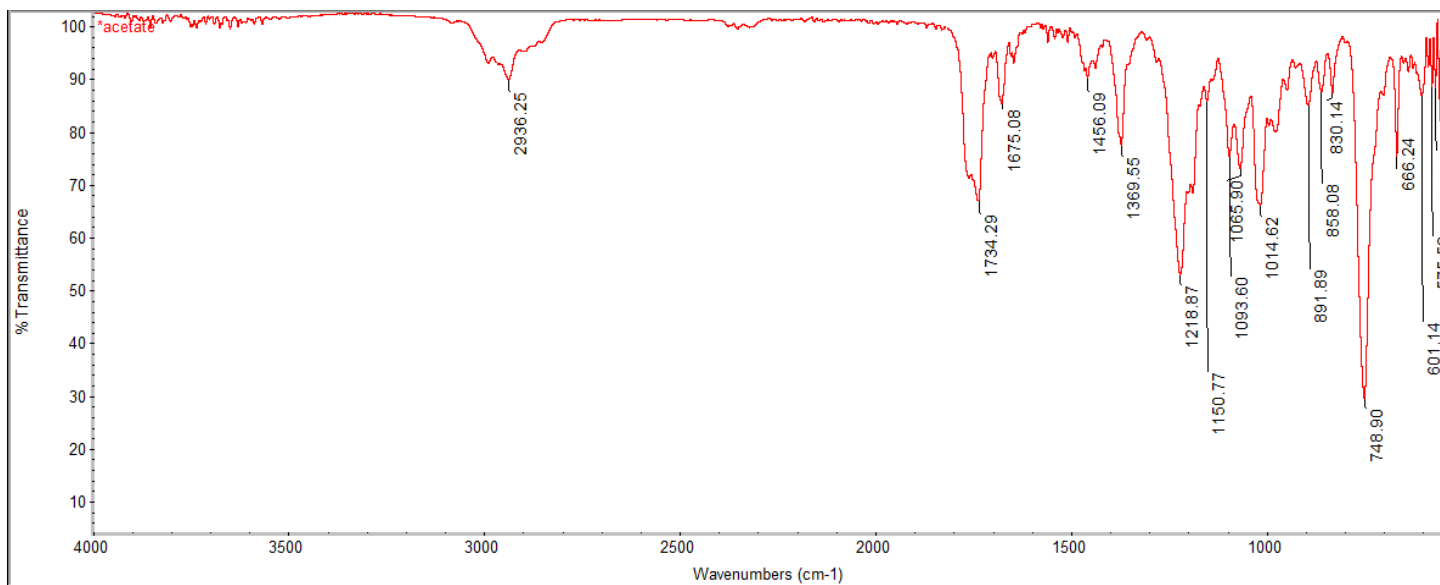


### Compound 3 (andrographolide acetate)

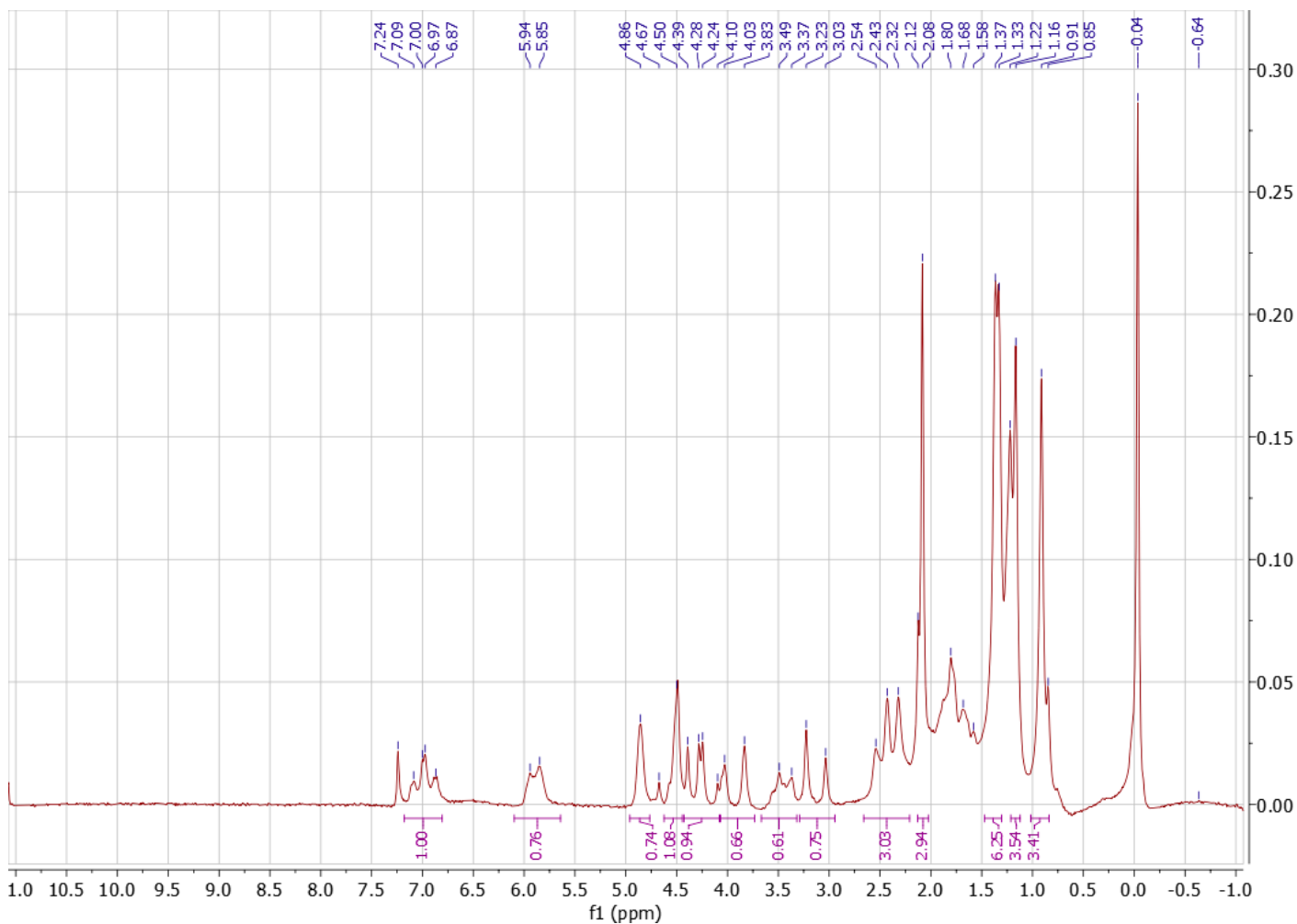
**Experimental procedure:** To an eight dram vial charged with a Teflon coated magnetic stir bar was added Compound **2** (1.00 g, 2.31 mmol, 1 eq.) in acetic anhydride (4.3 mL, 45.5 mmol, 20eq). The reaction mixture was heated and stirred at 80°C and monitored by thin-layer chromatography (85:15 ethyl acetate in hexanes). Full conversion of the starting material was observed after 60 minutes, upon which the crude reaction was directly loaded onto a column and purified via silica gel flash chromatography (0% to 50% ethyl acetate in hexanes, at a 10% gradient) to give the title compound **3** as an off-white gel in 75% isolated yield.

**Chemicals:** Andrographolide (95%) was purchased from AK Scientific and used without further purification. Acetic anhydride was purchased from JT Baker and used without further purification. Silica gel (230-400 mesh) was purchased from Merck, and solvents used in purification were purchased from Alliance Chemicals (ACS grade) and used without further purification.

**TLC**  $R_f = 0.75$  (50% EtOAc / 50% hexanes), green stain by PMA



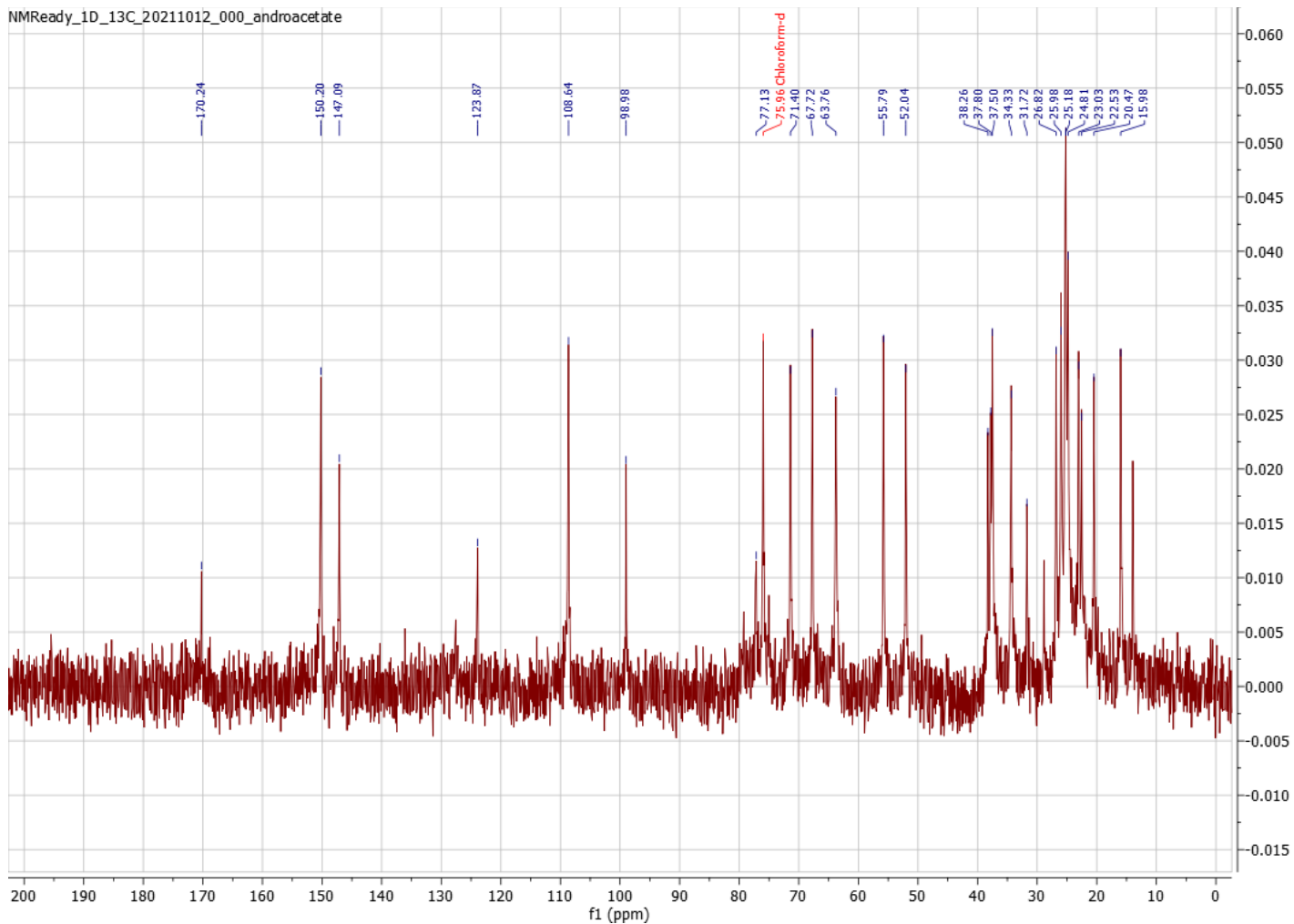
**FT-IR (neat, ATR):** 2936.25, 1743.29, 1676.08, 1456.09, 1369.56, 1218.87, 1150.77, 1093.60, 1065.90, 1014.82, 1014.62, 891.89, 858.08, 830.14, 666.24  $\text{cm}^{-1}$



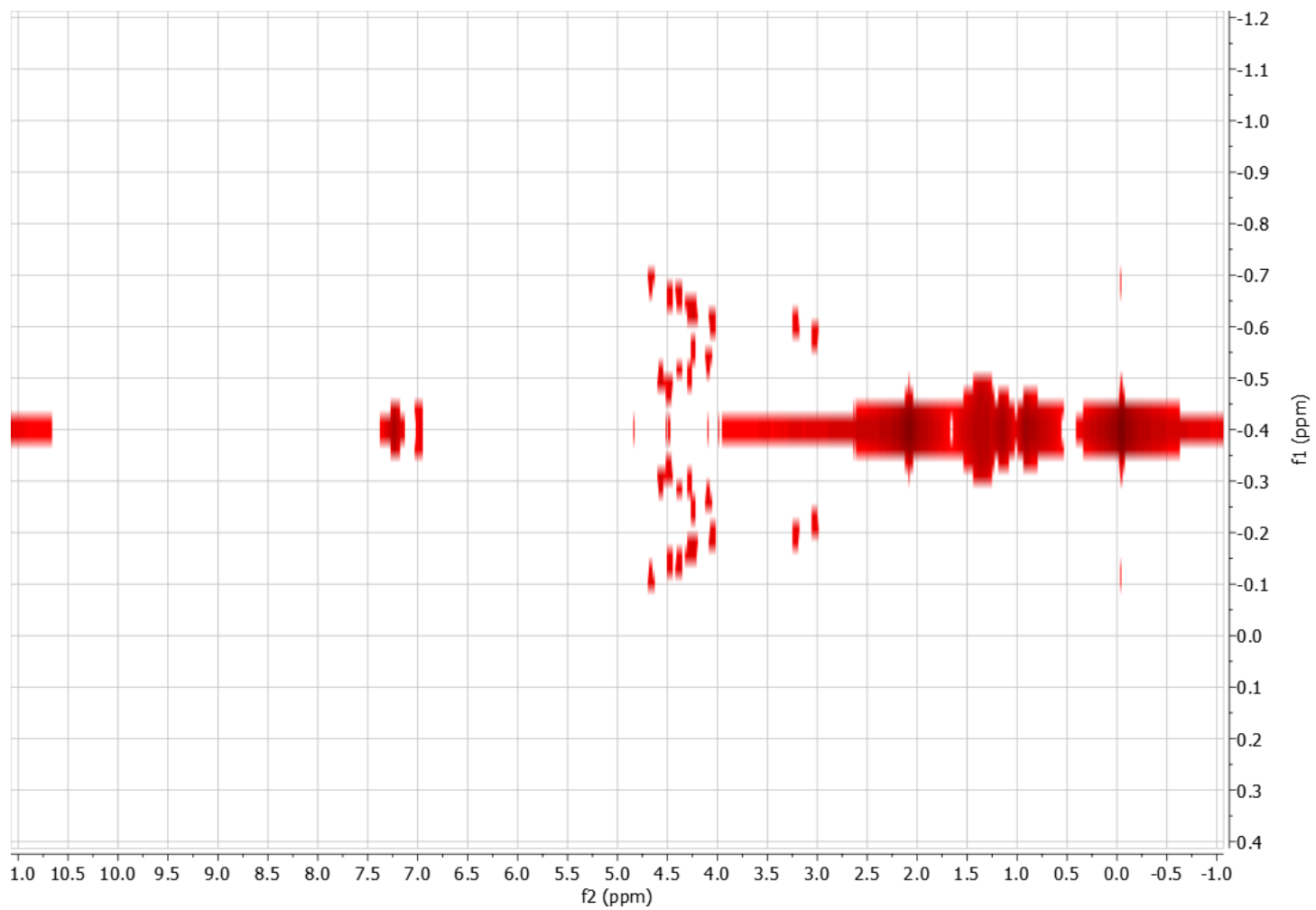
**$^1\text{H}$  NMR:** (60 MHz,  $\text{CDCl}_3$ )  $\delta$ , 7.01 (t,  $J = 6.7$  Hz, 1H, C12), 5.93 (dd,  $J = 5.9$  Hz, 1H, C14), 4.90 (m, 1H, C15a), 4.89 (s, 1H, C17a), 4.53 (s, 1H, C17b), 4.30 (dd,  $J = 6.4$  Hz, 1H, C15b), 3.97 (d,  $J = 11.8$  Hz, 1H, C19a), 3.46 (dd,  $J = 7.3$  Hz, 1H, C3), 3.17 (d,  $J = 11.6$  Hz, 1H, C19b), 2.41 (dd,  $J = 6.6$  Hz, 2H, C11),

1.97-1.83 (m, 4H, C2,7), 5.93 (d, J = 5.9 Hz, 1H, C14), 2.22 (s, 3H, acetate), 1.91-1.09 (m, 5H, C1,5,6), 1.47 (m, 1H, C9), 1.39-1.36 (3H, acetonide), 1.19 (s, 3H, C18), 0.95 (s, 3H, C20)

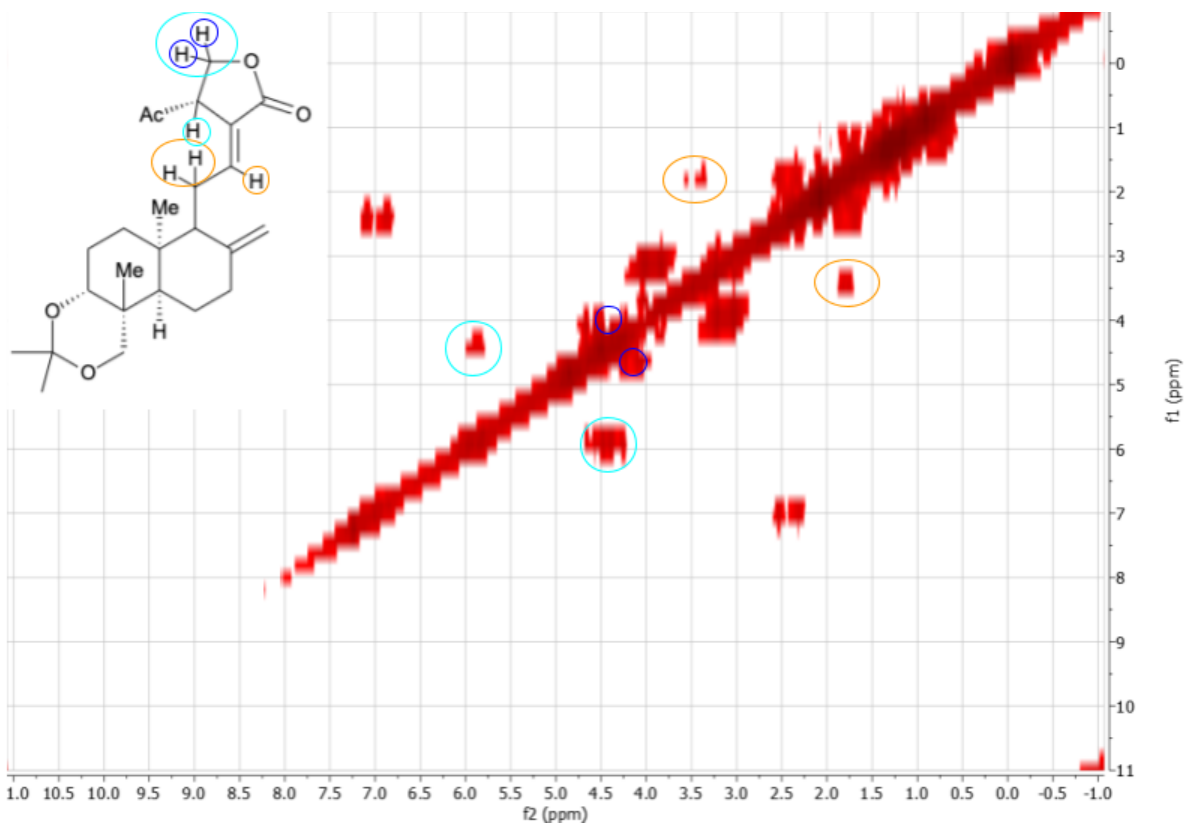
Carbon #	Observed	Literature Reported
C12	7.01 (t, J = 6.7 Hz, 1H),	7.00 (dd, J = 7.1, 1.8 Hz, 1H)
C14	5.93 (dd, J = 5.9 Hz, 1H),	5.93 (dd, J = 5.6, 2.5 Hz, 1H)
C15a	4.90 (m, 1H)	4.89–4.84 (m, 1H)
C17a	4.89 (s, 1H)	4.56 (s, 1H)
C17b	4.53 (s, 1H)	4.41 (s, 1H)
C15b	4.30 (dd, J = 6.4 Hz, 1H)	4.22 (dd, J = 11.3, 1.9 Hz, 1H),
C19a	3.97 (d, J = 11.8 Hz, 1H)	3.94 (d, J = 11.6 Hz, 1H)
C3	3.46 (dd, J = 7.3 Hz, 1H)	3.49 (dd, J = 8.4, 3.9 Hz, 1H)
C19b	3.17 (d, J = 11.6 Hz, 1H)	3.16 (d, J = 11.6 Hz, 1H)
C11	2.41 (dd, J = 6.6 Hz, 2H)	1.98 (dd, J = 12.2, 6.4 Hz, 2H)
C2, C7	1.97-1.83 (m, 4H)	2.10-1.47 (m, 4H)
C9	5.93 (d, J = 5.9 Hz, 1H)	2.55–2.31 (m, 3H)
Acetate	2.22 (s, 3H, acetate)	1.39 (s, 3H)
C1, C5, C6	1.91-1.09 (m, 5H, C1,5,6)	1.91–1.83 (m, 2H) 1.83–1.64 (m, 3H)
Acetonide	1.39-1.36 (m, 6H, acetonide)	1.28 (tdd, J = 12.5, 8.2, 4.6 Hz, 3H) 1.35 (s, 3H)
C18	1.19 (s, 3H)	1.18 (s, 3H)
C20	0.95 (s, 3H)	0.94 (s, 3H)



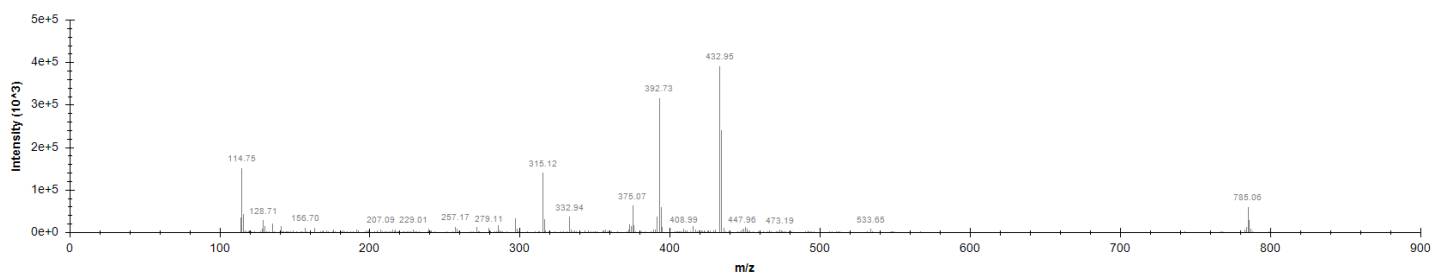
<sup>13</sup>C NMR (15 MHz, CDCl<sub>3</sub>) δ 170.24, 150.20, 147.09, 123.87, 108.64, 98.98, 77.13, 71.40, 67.72, 63.76, 55.79, 52.04, 38.26, 37.80, 37.50, 34.33, 31.72, 26.82, 25.98, 25.18, 24.81, 23.03, 22.53, 20.47, 15.98.



**JRES**

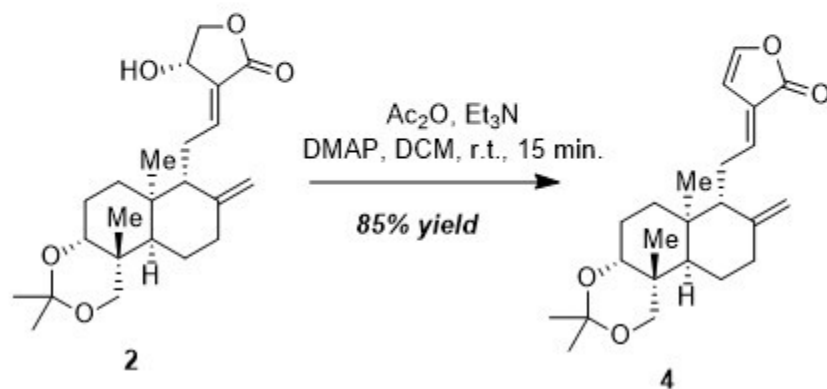


$^1\text{H}$ - $^1\text{H}$  COSY NMR



ESI-MS ( $m/z$ ):  $[\text{M}+\text{H}]^+$  calc'd for  $\text{C}_{25}\text{H}_{36}\text{O}_6^+$  : 432.25, found: 432.95

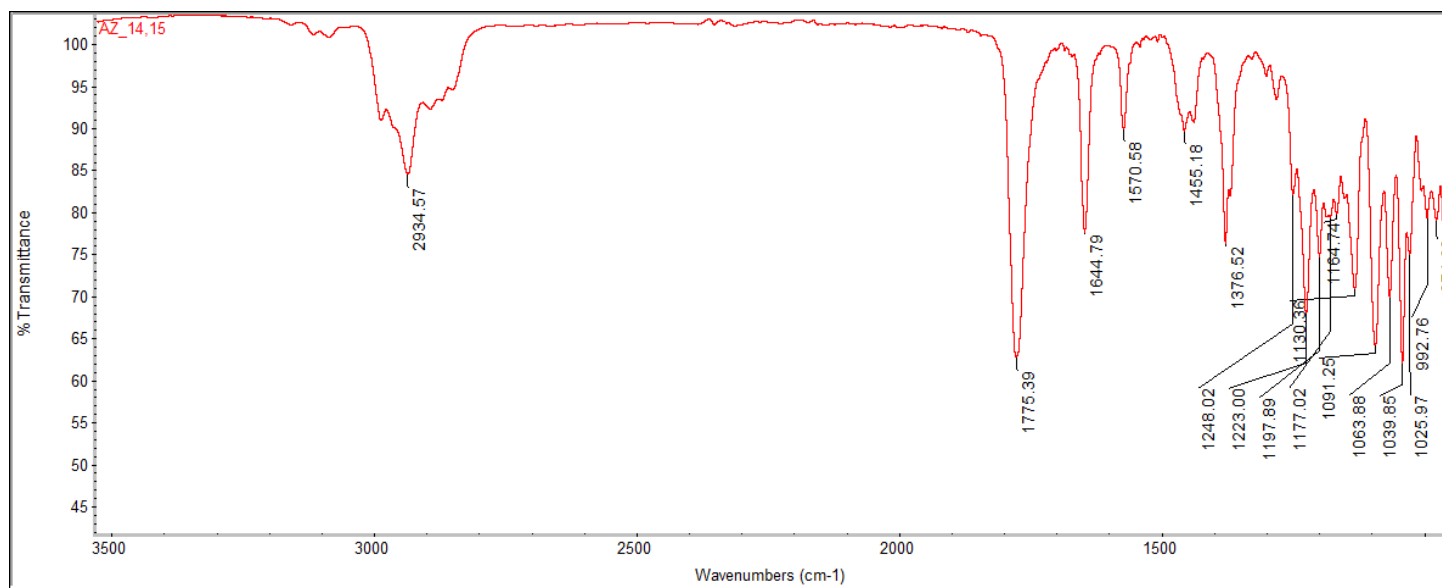
## Compound 4 (14, 15 elimination product)



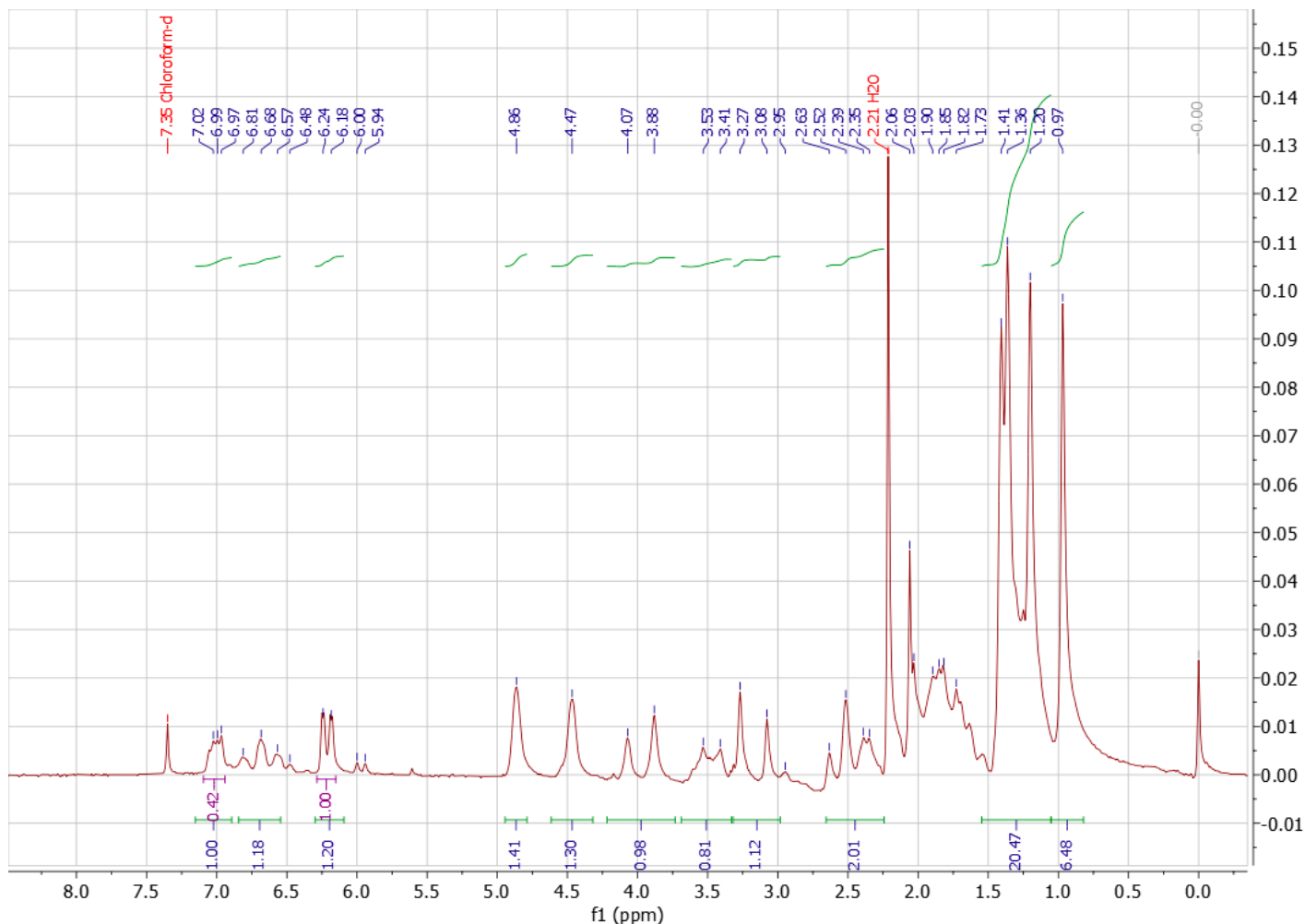
**Experimental procedure:** To a 50 mL round bottom flask charged with a Teflon coated magnetic stir bar was added andrographolide acetonide **2** (680 mg, 1.74 mmol, 1 eq.) in methylene chloride (5.2 mL). To this was sequentially added acetic anhydride (980  $\mu\text{L}$ , 10.4 mmol, 6 eq.), triethylamine (1.00 mL, 7.8 mmol, 4.5 eq.) and DMAP (288 mg, 2.36 mmol, 1.35 eq.). The reaction was stirred for fifteen minutes upon which full conversion of starting material was observed by thin layer chromatography. The reaction material was directly flushed through flash chromatography whereby an eluent of 25% ethyl acetate in hexanes afforded alkene **4** (590 mg, 81% yield) as a off-white solid.

**Chemicals:** Andrographolide (95%) was purchased from AK Scientific and used without further purification. Triethylamine (99.5%) was purchased from Sigma Aldrich, 4-dimethylaminopyridine (DMAP) (95%) was purchased from AK Scientific, and acetic anhydride (99%) was purchased from JT Baker. Methylene chloride (ACS grade) was purchased from Stellar Chemical. Silica gel (230-400 mesh) was purchased from Merck, and solvents used in purification were purchased from Alliance Chemicals (ACS grade) and used without further purification.

**TLC**  $R_f$  = 0.60 (50% EtOAc / 50% hexanes), green stain by PMA



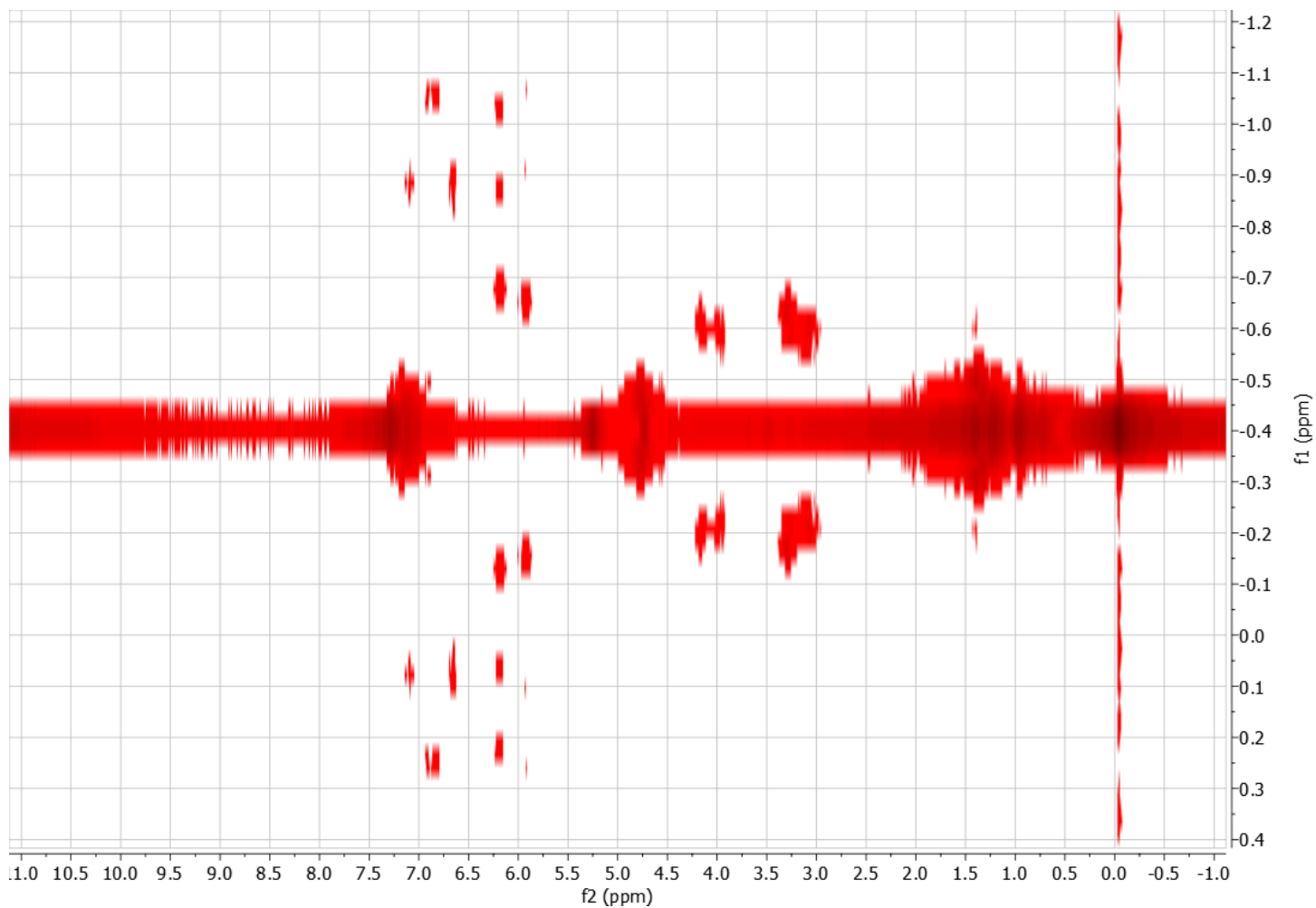
**FT-IR (neat, ATR):** 2934.57, 1775.39, 1644.79, 1570.58, 1455.16, 1376.52, 1248.02, 1223.00, 1197.89, 1177.02, 1130.36, 1091.25, 1164.74, 1063.66, 1039.66, 1025.97, 992.75  $\text{cm}^{-1}$

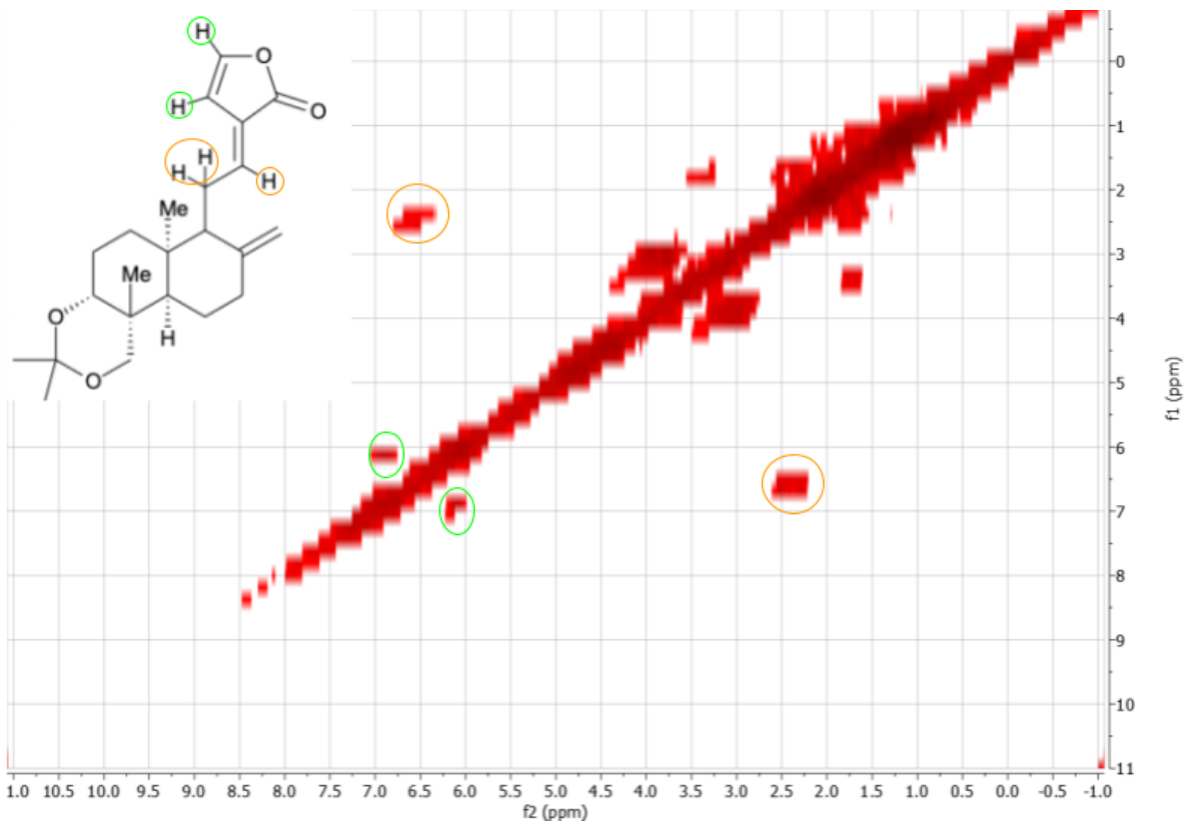


**<sup>1</sup>H NMR** (60 MHz, CDCl<sub>3</sub>) δ 6.91 (dd, J = 16.29, 9.70Hz, 1H, C11), 6.81 (d, J = 3.6, 1H, C15), 6.21 (dd, 1H, J = 0.8, 3.5 Hz, C14), 6.11 (d, J = 15.81 Hz, 1H, C12), 4.86 (s, 1H, C17a), 4.46 (s, 1H, C17b), 3.97 (d, J = 11.56Hz, 1H, C19a), 3.13 (d, J = 11.11 Hz, 1H, C19b), 3.50 (dd, J = 4.89, 10.94 Hz, 1H, C3), 2.35 (d, J = 11.00 Hz, 1H, C9), 1.19 (s, 3H, C18), 0.96 (s, 3H, C20), 1.41-1.36 (Acetonide, 6H)

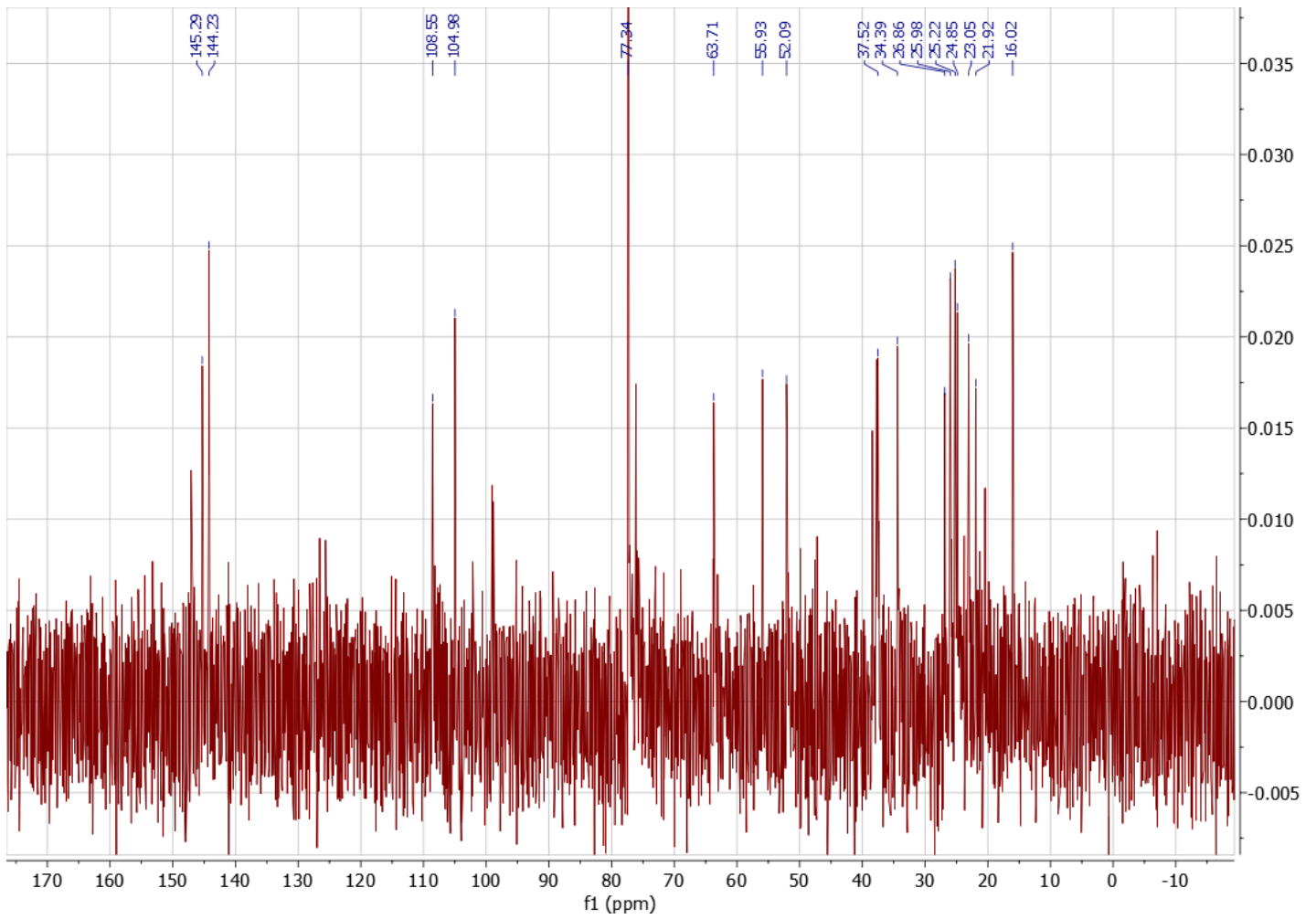
Carbon #	Observed	Literature Reported
	7.38 (s, 1H)	7.65 (s, 1H)
C11	6.91 (dd, J = 16.29, 9.70Hz, 1H)	6.74 (dd, J = 15.78, 9.96 Hz, 1H)
C15	6.81 (d, J = 3.6, 1H)	6.12 (d, J = 15.78 Hz, 1H)
C14	6.21 (dd, 1H, J = 0.8, 3.5 Hz)	5.04 (d, J = 4.98Hz, 1H)
C12	6.11 (d, J = 15.81 Hz, 1H)	4.89 (s, 2H)
C17a	4.86 (s, 1H)	4.73 (s, 1H)
C17b	4.46 (s, 1H)	4.42 (s, 1H)

		4.14 (dd, J = 7.62, 2.64 Hz, 1H)
		3.85 (dd, J = 10.8, 2.61 Hz, 1H)
		3.28 – 3.19 (m, 2H)
		2.36 (d, J = 10.53 Hz, 2H)
		2.01 – 1.16 (m, 8H)
C18	1.19 (s, 3H)	1.09 (s, 3H)
C20	0.96 (s, 3H)	0.76 (s, 3H)

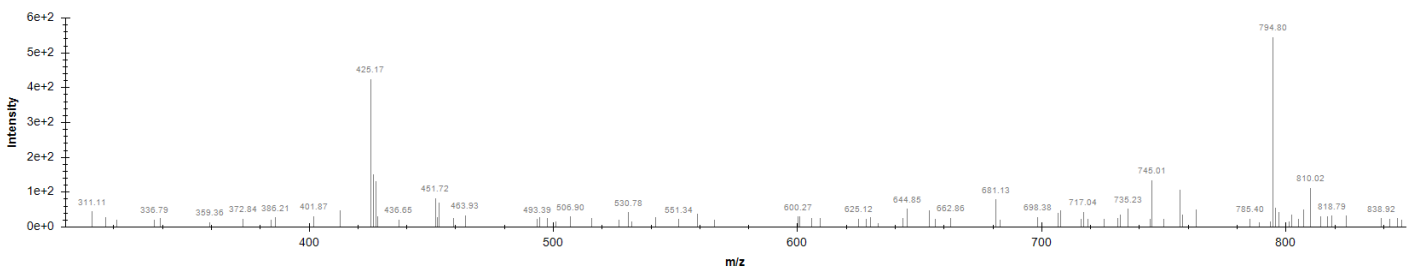




$^1\text{H}$ - $^1\text{H}$  COSY NMR

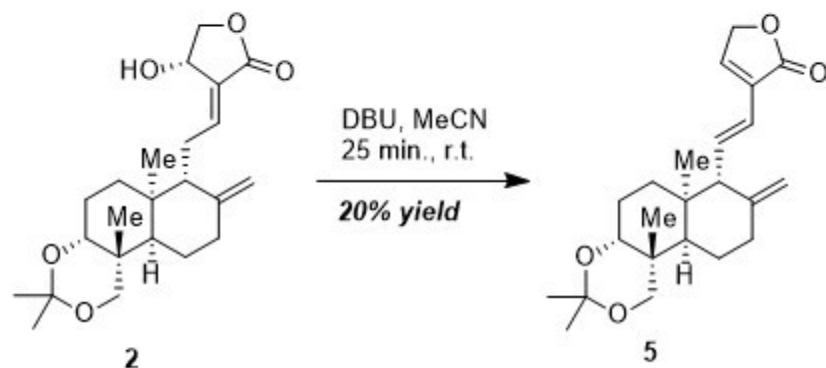


$^{13}\text{C}$  NMR (15 MHz,  $\text{CDCl}_3$ )  $\delta$  146.91, 145.29, 144.23, 108.55, 104.98, 77.34, 63.71, 55.93, 52.09, 37.52, 34.39, 26.86, 25.98, 25.22, 24.85, 23.06, 21.92, 20.26, 16.02



ESI-MS (m/z):  $[\text{M}+\text{H}]^+$  calc'd for  $\text{C}_{23}\text{H}_{33}\text{O}_4^+$ : 373.2379, found as a dimer  $[2\text{M}-\text{H}]^+$ : 745.21

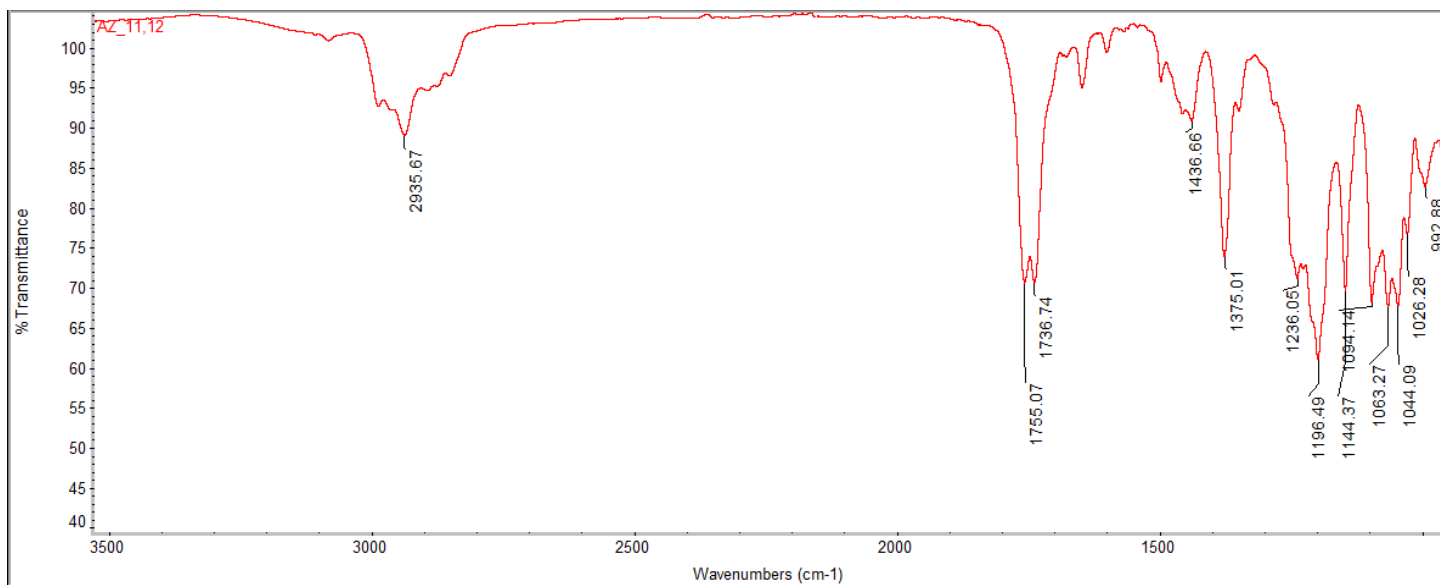
## Compound 5 (11, 12 elimination product)



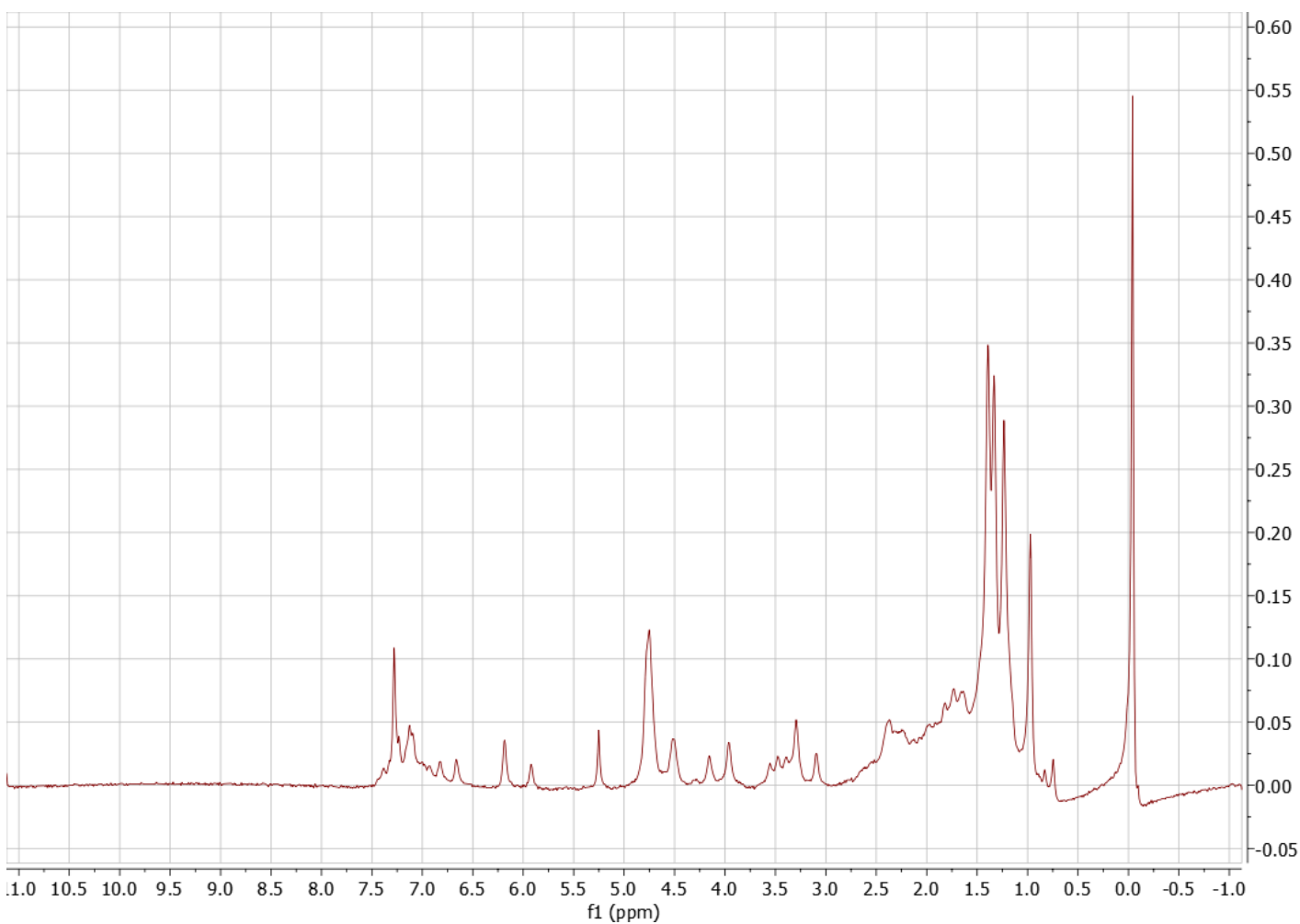
**Experimental procedure:** To a 50 mL round bottom flask charged with a Teflon coated magnetic stir bar was added andrographolide acetonide **2** (100 mg, 0.268 mmol, 1 eq.) in acetonitrile at a 5.36 mM solution. To this, DBU (490  $\mu$ L, 3.28 mmol, 5 eq.) was added dropwise. The reaction mixture was stirred at ambient temperature with a magnetic stir plate, and monitored by thin-layer chromatography (30:70 ethyl acetate in hexanes). Full conversion of the starting material was observed after 40 minutes, upon which the crude reaction was quenched in brine, and concentrated *in vacuo*. The resulting crude material was taken up in DCM, loaded onto a column, and purified via silica gel flash chromatography (10% to 50% ethyl acetate in hexanes, at a 10% gradient) to give the title compound **5** as an off-white solid in 20% isolated yield.

**Chemicals:** Andrographolide (95%) was purchased from AK Scientific and used without further purification. HPLC grade Acetone was purchased from J.T. Baker. 2,2-dimethoxypropane (95%) and PPTS (95%) was also purchased from AK Scientific and used without further purification. Methylene chloride (ACS grade) was purchased from Stellar Chemical. Silica gel (230-400 mesh) was purchased from Merck, and solvents used in purification were purchased from Alliance Chemicals (ACS grade) and used without further purification.

**TLC**  $R_f$  = 0.60 (50% EtOAc / 50% hexanes), green stain by PMA

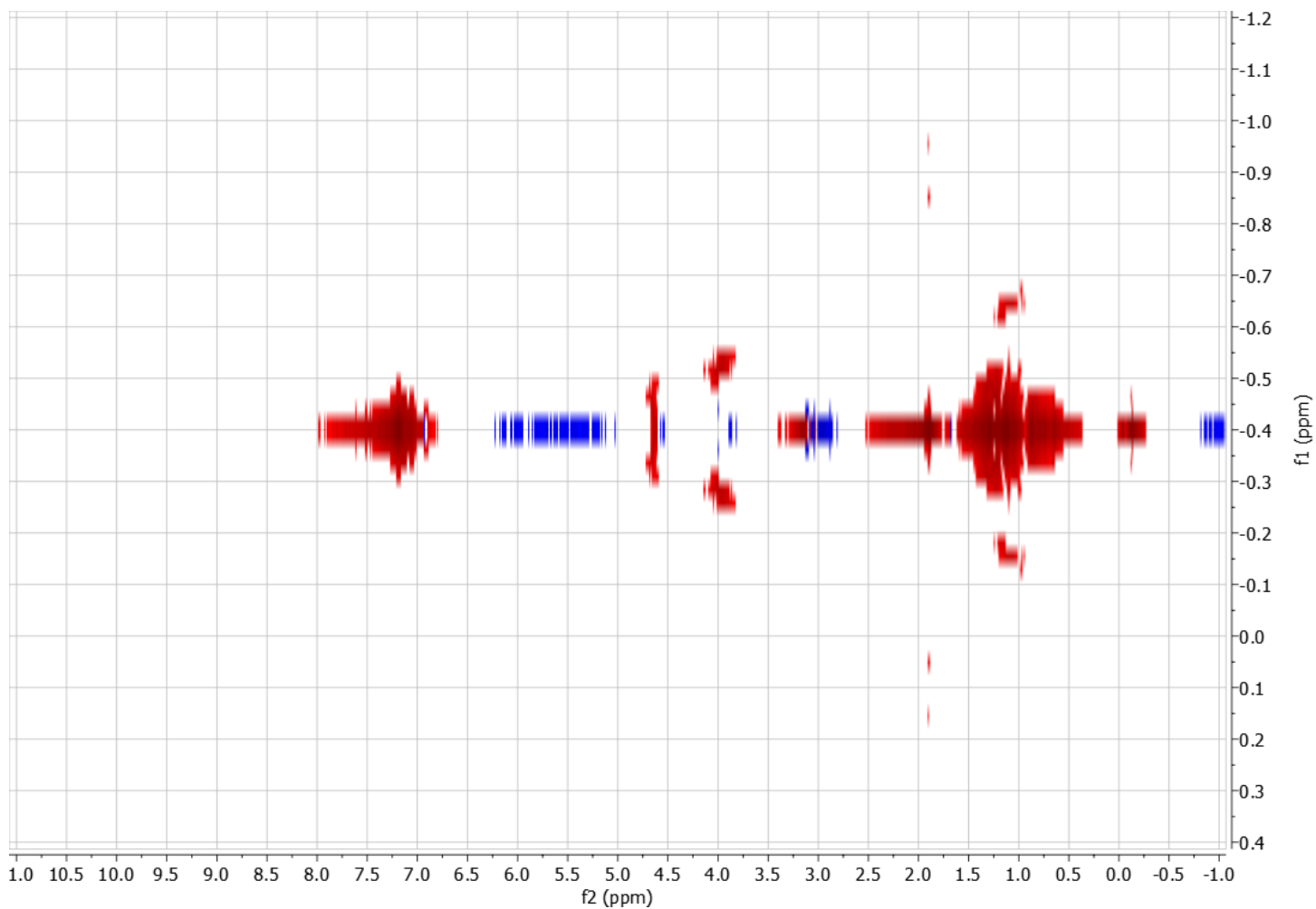


**FT-IR (neat, ATR):** 2935.67, 1755.07, 1736.74, 1436.66, 1375.01, 1236.05, 1196.49, 1144.37, 1094.14, 1063.27, 1044.09, 1026.28, 992.88  $\text{cm}^{-1}$

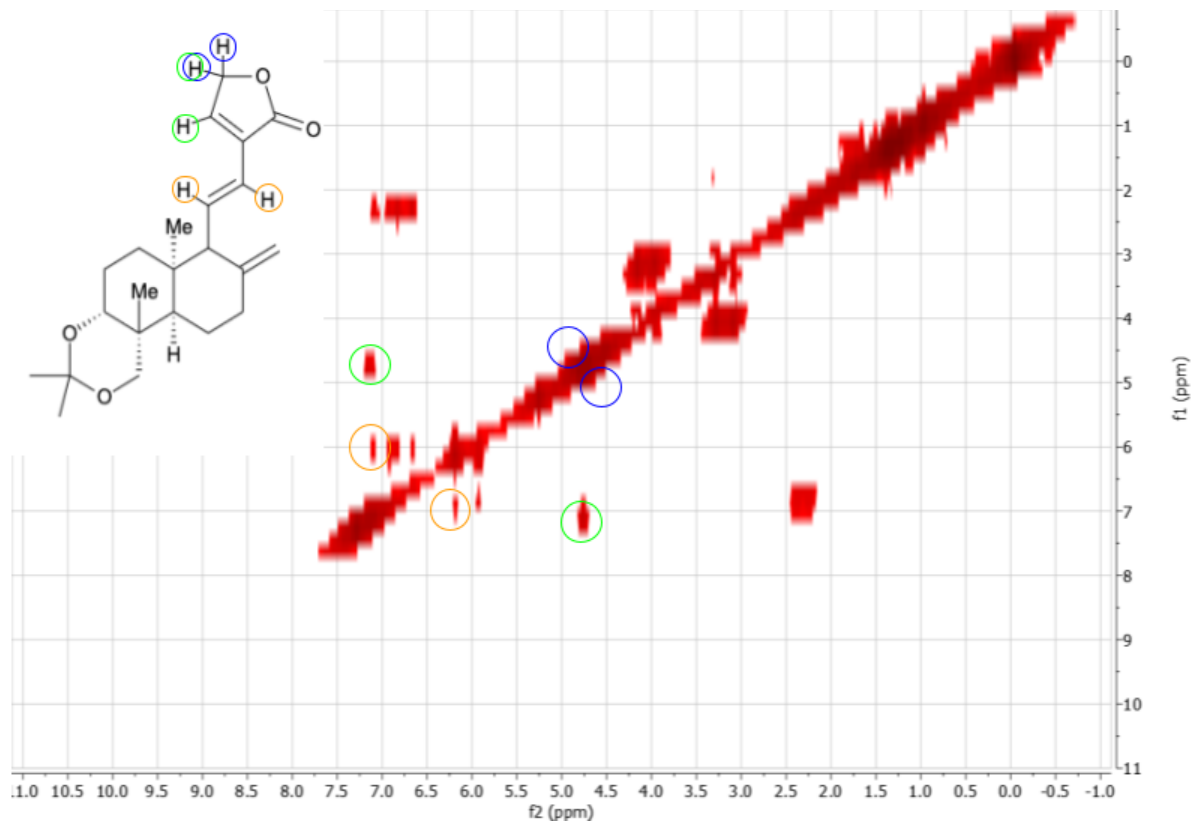


**$^1\text{H}$  NMR (60 MHz,  $\text{CDCl}_3$ )  $\delta$ ,** 7.34 (s, 1H, C14), 7.11 (dd,  $J = 15.8\text{Hz}, 10\text{Hz}$ , 1H, C11), 6.41 (d,  $J = 15.8\text{Hz}$ , 1H, C12), 4.99 (s, 2H, C15), 4.94 (s, 1H, C17a), 4.73 (s, 1H, C17b), 2.48 (d,  $J = 10.2\text{Hz}$ , 1H, C9), 2.40-1.40 (m, 7H, C1,5,6,7), 1.96 (m, 2H, C2), 1.58-1.64 (3H, Acetonide), 1.48 (s, 3H, C18), 1.21 (s, 3H, C20)

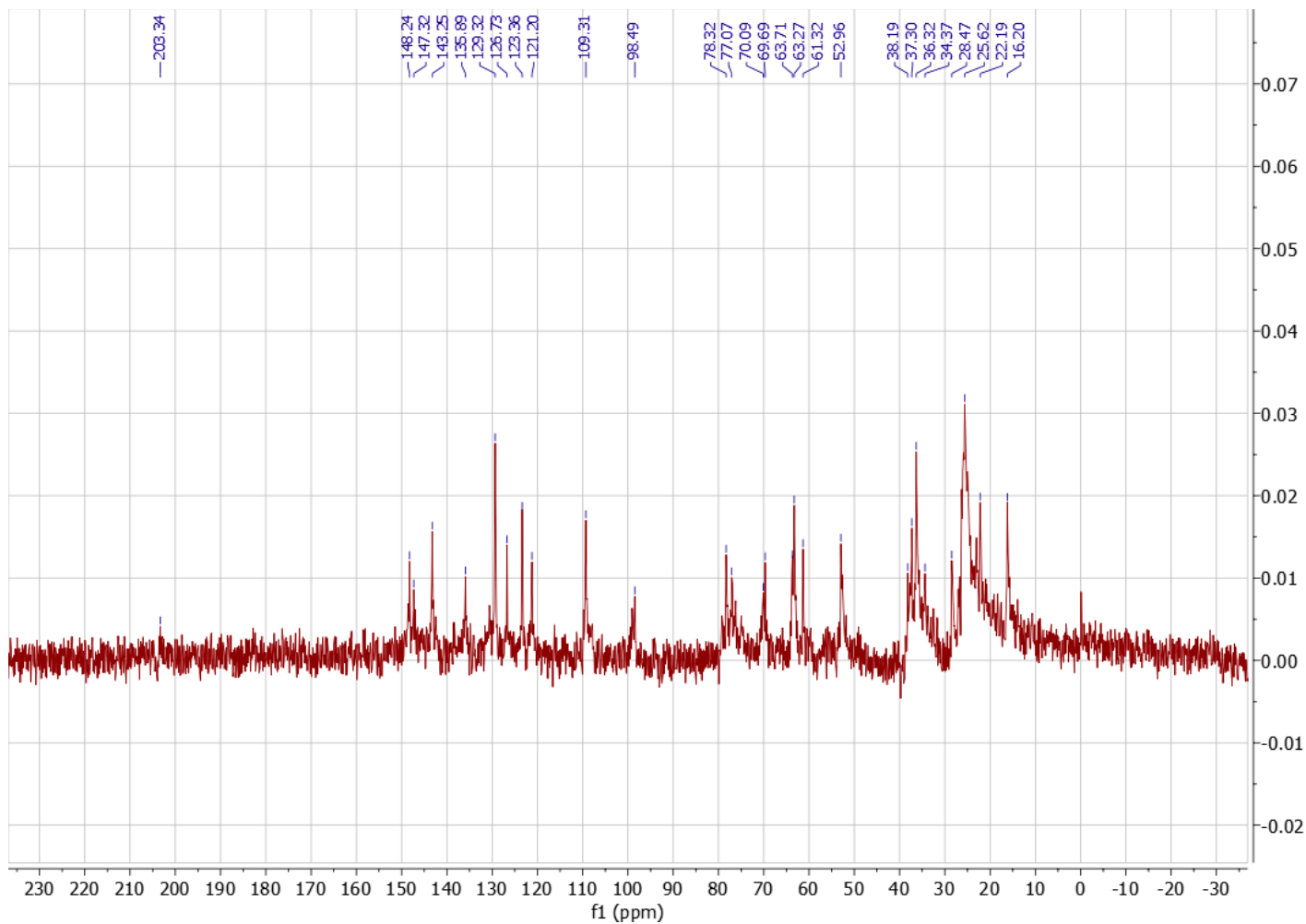
Carbon #	Observed	Literature Reported
C14	7.34 (s, 1H)	7.45 (1H, s)
C11	7.11 (dd, J = 15.8Hz, 10Hz, 1H)	6.89 (1H, dd, J = 10, 15.7Hz)
C12	6.41 (d, J = 15.8Hz, 1H)	6.17 (1H, d, J = 15.9Hz)
C15a	4.99 (s, 2H, C15)	4.76 (1H, s)
C15b		
C17a	4.94 (s, 1H, C17a)	4.60 (1H, s)
C17b	4.73 (s, 1H, C17b)	4.50 (1H, s)



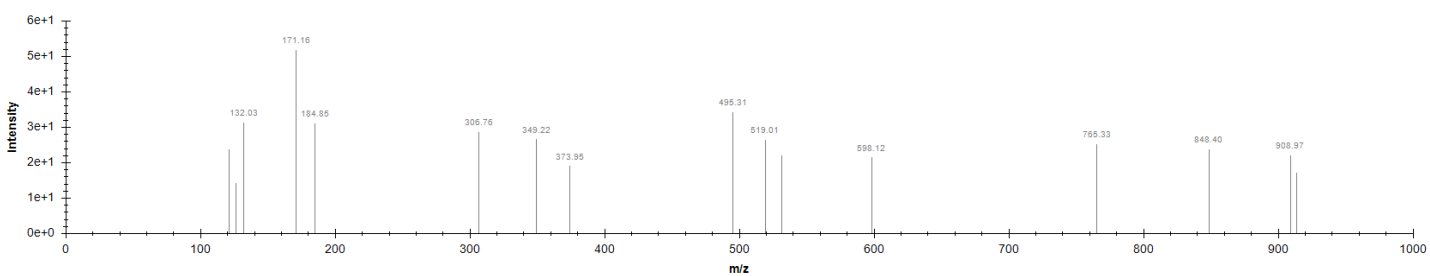
**JRES**



$^1\text{H}$ - $^1\text{H}$  COSY NMR



$^{13}\text{C}$  NMR (15 MHz,  $\text{CDCl}_3$ )  $\delta$  148.24, 147.32, 143.25, 136.89, 129.32, 126.73, 123.36, 121.20, 109.31, 98.49, 78.32, 77.07, 70.09, 69.69, 63.71, 63.27, 61.32, 52.96, 38.19, 37.30, 36.32, 34.37, 28.47, 25.62, 22.19, 16.20

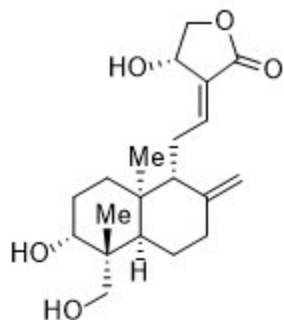


ESI-MS (m/z):  $[\text{M}+\text{H}]^+$  calc'd for  $\text{C}_{23}\text{H}_{33}\text{O}_4^+$ : 373.2379, found: 373.95

### 3. DFT Optimized Structures

#### Compound 1

DFT-optimized structure (B3LYP 6-31G)



andrographolide (1)

\* xyz 0 1

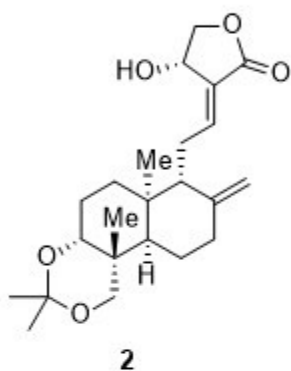
H	1.31610	-0.37729	0.23568
C	2.36443	-0.25537	-0.08855
C	2.59995	-1.41230	-1.09390
C	2.65471	-2.80091	-0.44973
C	2.03957	-2.79261	0.91688
C	0.95561	-3.53134	1.20870
C	2.68407	-1.84692	1.93174
H	1.87853	-1.56785	2.62763
C	3.71599	-2.66943	2.76232
C	4.14682	-2.05515	4.06909
C	4.85345	-2.67491	5.02938
C	5.27809	-2.08402	6.32202
H	4.54871	-1.40025	6.76489
O	6.50409	-1.37788	6.14911
C	5.46963	-3.32310	7.16871
O	5.81065	-4.37294	6.25507
C	5.32976	-4.07923	5.01334
O	5.34722	-4.83482	4.06195
C	3.19502	-0.48261	1.24211
C	4.71459	-0.53864	0.96261
C	2.92026	0.69447	2.22168
C	3.01094	2.07966	1.59859
C	2.06217	2.21857	0.41321
H	1.03958	2.05115	0.77599
O	2.08652	3.56517	-0.06131
C	2.36250	1.19891	-0.72466
C	1.19176	1.28849	-1.74747
C	3.63725	1.63960	-1.49337
O	3.96630	0.77369	-2.56820
H	3.53382	-1.28263	-1.64498
H	1.79643	-1.41378	-1.83943
H	3.69539	-3.13695	-0.36692

H	2.16618	-3.52534	-1.11304
H	0.49762	-4.18315	0.47043
H	0.50118	-3.51053	2.19435
H	3.26026	-3.64043	3.00125
H	4.59990	-2.88887	2.15211
H	3.86552	-1.02471	4.25387
H	7.13955	-1.96662	5.70287
H	4.55274	-3.61506	7.69280
H	6.28191	-3.21231	7.89353
H	4.99035	-1.36986	0.30904
H	5.28809	-0.64686	1.88905
H	5.09079	0.37177	0.50061
H	3.61752	0.66741	3.06385
H	1.91449	0.59093	2.64955
H	4.04164	2.31162	1.30896
H	2.75374	2.83274	2.35478
H	2.96459	3.94605	0.10670
H	0.23814	1.00964	-1.28513
H	1.34761	0.63284	-2.60981
H	1.07869	2.30674	-2.13722
H	3.48650	2.63321	-1.93248
H	4.50934	1.72448	-0.84650
H	4.71061	1.17657	-3.04718

\*

**Compound 2**

DFT-optimized structure (B3LYP 6-31G)



\* xyz 0 1

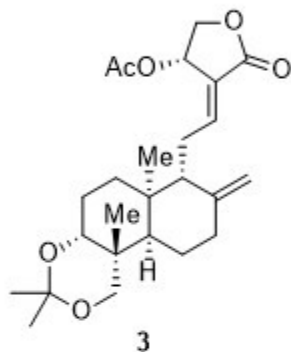
H	1.49274	-0.17951	-0.62903
C	2.56991	-0.15658	-0.41399
C	3.11209	1.03427	-1.24157
C	2.42831	2.35515	-0.87735
C	2.44637	2.60696	0.60799
C	2.93904	3.74132	1.13219
C	1.89058	1.47874	1.47634
H	2.10682	1.72185	2.52767
C	0.33727	1.47646	1.34257
C	-0.38442	0.81276	2.48817
C	-1.51610	0.09136	2.41024
C	-2.17252	-0.66885	3.50552
H	-2.90385	-0.03630	4.02039
O	-1.25679	-1.19330	4.45389
C	-2.86049	-1.76067	2.71611
O	-3.17584	-1.19220	1.44581
C	-2.33998	-0.14355	1.19637
O	-2.33191	0.51081	0.17149
C	2.67276	0.13491	1.13730
C	4.13488	0.36017	1.63200
C	2.10962	-1.07434	1.92260
C	2.71024	-2.41828	1.49819
C	2.49340	-2.67915	0.00573
H	2.93667	-3.65368	-0.23229
O	1.07510	-2.77415	-0.17072
C	0.64637	-2.95548	-1.51774
C	0.90877	-4.38338	-2.00818
C	-0.86502	-2.71449	-1.51034
O	1.19126	-1.97503	-2.39591
C	2.60451	-1.88418	-2.32898
C	3.09629	-1.57044	-0.89315
C	4.63288	-1.67974	-0.94149
H	2.94810	0.86824	-2.31063
H	4.19442	1.13847	-1.11144

H	1.38806	2.33590	-1.22463
H	2.91923	3.16999	-1.42325
H	3.33634	4.53173	0.50234
H	2.95471	3.91333	2.20401
H	-0.01633	2.51660	1.32459
H	0.04907	1.03351	0.38649
H	0.08044	0.92620	3.46687
H	-0.49868	-1.56317	3.96715
H	-3.78437	-2.08148	3.20835
H	-2.23407	-2.64894	2.57061
H	4.69141	1.07125	1.01643
H	4.72271	-0.55474	1.68342
H	4.13525	0.75594	2.65561
H	1.03156	-1.15428	1.76788
H	2.26089	-0.93345	3.00000
H	2.20789	-3.20486	2.07615
H	3.77160	-2.47928	1.75403
H	1.97405	-4.63143	-2.01442
H	0.54750	-4.51889	-3.03328
H	0.42311	-5.11709	-1.35561
H	-1.08439	-1.69327	-1.17866
H	-1.37774	-3.39459	-0.82154
H	-1.29386	-2.82507	-2.51218
H	2.91998	-1.11443	-3.03909
H	3.04035	-2.81747	-2.70573
H	5.07233	-0.91591	-1.59063
H	4.93795	-2.65231	-1.34771
H	5.10669	-1.60643	0.03445

\*

### Compound 3

DFT-optimized structure (B3LYP 6-31G)



\* xyz 0 1

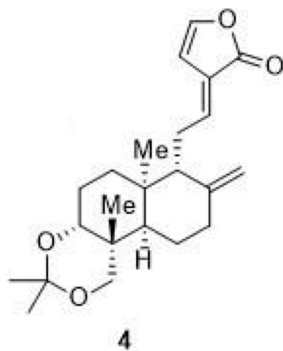
H	0.23591	-0.65997	-0.51233
C	1.30993	-0.63862	-0.28146
C	1.87777	0.50435	-1.15731
C	1.19836	1.84610	-0.87084
C	1.20089	2.17311	0.59961
C	1.69797	3.32855	1.07101
C	0.62389	1.09582	1.51731
H	0.83514	1.39011	2.55652
C	-0.92839	1.10298	1.37252
C	-1.65939	0.52063	2.55639
C	-2.79617	-0.19683	2.52319
C	-3.45609	-0.89549	3.66230
H	-4.18254	-0.21526	4.12583
C	-4.13032	-2.03205	2.92094
O	-4.44697	-1.53186	1.62211
C	-3.61416	-0.49623	1.32160
O	-3.60941	0.10968	0.26713
O	-2.48979	-1.34712	4.61530
C	-3.01685	-1.90712	5.73534
C	-1.92195	-2.34122	6.66005
O	-4.21057	-2.05019	5.95275
C	1.39144	-0.27371	1.25560
C	2.84798	-0.04460	1.76378
C	0.79675	-1.43664	2.08695
C	1.38345	-2.80807	1.73732
C	1.19146	-3.13624	0.25452
H	1.62485	-4.12693	0.07118
O	-0.22380	-3.21975	0.05315
C	-0.63087	-3.45489	-1.29180
C	-0.38596	-4.90847	-1.71035
C	-2.13729	-3.18617	-1.32466
O	-0.05152	-2.52703	-2.20484
C	1.36123	-2.45576	-2.11180

C	1.82782	-2.07959	-0.68278
C	3.36344	-2.21045	-0.69369
H	1.73072	0.28693	-2.21956
H	2.95853	0.60624	-1.01312
H	0.16211	1.81524	-1.22917
H	1.70131	2.62872	-1.45178
H	2.11006	4.08186	0.40616
H	1.70235	3.55543	2.13257
H	-1.27111	2.14322	1.28624
H	-1.21555	0.60157	0.44534
H	-1.18539	0.67913	3.52363
H	-5.05761	-2.33749	3.41601
H	-3.49454	-2.92015	2.82219
H	-1.31352	-3.11004	6.17718
H	-2.36070	-2.76137	7.56951
H	-1.30690	-1.48116	6.93655
H	3.42460	0.62755	1.12345
H	3.42111	-0.96394	1.87095
H	2.83745	0.40125	2.76654
H	-0.27969	-1.50830	1.91655
H	0.93160	-1.24711	3.15907
H	0.85770	-3.55889	2.34146
H	2.43860	-2.87254	2.01700
H	0.67438	-5.17555	-1.68218
H	-0.72872	-5.08492	-2.73556
H	-0.89865	-5.60222	-1.03513
H	-2.34362	-2.14747	-1.04186
H	-2.67577	-3.82594	-0.61714
H	-2.54908	-3.33292	-2.32901
H	1.70500	-1.72733	-2.85175
H	1.78883	-3.41346	-2.43267
H	3.82697	-1.47874	-1.36270
H	3.66368	-3.20232	-1.05430
H	3.81774	-2.10524	0.28858

\*

## Compound 4

DFT-optimized structure (B3LYP 6-31G)



\* xyz 0 1

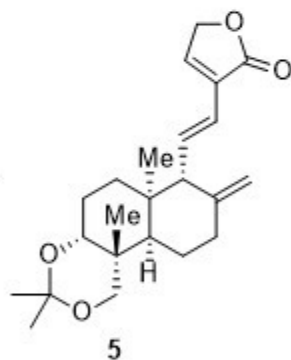
H	1.53234	-0.14813	-0.56638
C	2.61755	-0.08130	-0.40739
C	3.05528	1.16355	-1.21592
C	2.32175	2.42968	-0.76682
C	2.42391	2.63480	0.72148
C	2.89557	3.77515	1.25213
C	1.98051	1.45357	1.58334
H	2.26320	1.67570	2.62341
C	0.42408	1.37375	1.56253
C	-0.17439	0.74263	2.79655
C	-1.29538	0.00902	2.85015
C	-1.80998	-0.62002	4.02008
C	-2.90570	-1.24964	3.61768
O	-3.23548	-1.12186	2.27055
C	-2.24879	-0.30803	1.74077
O	-2.21444	0.09150	0.59120
C	2.79120	0.15657	1.14749
C	4.26757	0.41972	1.57436
C	2.30852	-1.10162	1.90934
C	2.93489	-2.40523	1.40251
C	2.66633	-2.61672	-0.08991
H	3.13980	-3.56096	-0.38513
O	1.24836	-2.76630	-0.21396
C	0.76810	-2.91241	-1.54679
C	1.06665	-4.30785	-2.10556
C	-0.74997	-2.73642	-1.46649
O	1.23392	-1.87682	-2.40803
C	2.64354	-1.72864	-2.39375
C	3.18285	-1.44943	-0.96779
C	4.71907	-1.48975	-1.08568
H	2.84360	1.02740	-2.28073
H	4.13602	1.32104	-1.13638
H	1.26351	2.35904	-1.04687
H	2.72880	3.28831	-1.31448

H	3.21358	4.60330	0.62575
H	2.97367	3.91387	2.32597
H	0.01652	2.39314	1.51944
H	0.09018	0.86560	0.65540
H	0.37631	0.90684	3.72085
H	-1.39208	-0.59959	5.01199
H	-3.59114	-1.85416	4.18797
H	4.76426	1.17102	0.95531
H	4.88909	-0.47392	1.56558
H	4.30850	0.78163	2.60960
H	1.22557	-1.21099	1.80615
H	2.51021	-0.99713	2.98265
H	2.48606	-3.23213	1.96805
H	4.00779	-2.43698	1.61181
H	2.13986	-4.51036	-2.16569
H	0.66740	-4.41839	-3.11950
H	0.63958	-5.08628	-1.46389
H	-0.99620	-1.74034	-1.08160
H	-1.20433	-3.46603	-0.78749
H	-1.21679	-2.82320	-2.45360
H	2.89810	-0.92036	-3.08526
H	3.10056	-2.62773	-2.82472
H	5.09896	-0.67110	-1.70474
H	5.04526	-2.42302	-1.56178
H	5.23197	-1.45575	-0.12759

\*

**Compound 5**

DFT-optimized structure (B3LYP 6-31G)



\* xyz 0 1

H	1.17225	0.16182	-0.14615
C	2.27284	0.12753	-0.15344
C	2.71548	1.37767	-0.95599
C	2.28463	2.69152	-0.30415
C	2.65805	2.73592	1.15633
C	3.42890	3.71036	1.66943
C	2.08656	1.57934	2.00335
H	2.51512	1.65973	3.01444
C	0.61370	1.92818	2.22344
C	-0.59036	1.37570	2.42179
C	-1.08447	0.04929	2.60151
C	-0.76557	-0.86068	3.51980
C	-1.61847	-2.05520	3.39871
O	-2.57345	-1.71519	2.39948
C	-2.30311	-0.46262	1.93637
O	-2.98798	0.14865	1.13367
C	2.69547	0.24688	1.36617
C	4.24633	0.34704	1.57120
C	2.24571	-1.01754	2.11371
C	2.69586	-2.32948	1.46589
C	2.20901	-2.43780	0.01890
H	2.60071	-3.37904	-0.38503
O	0.78190	-2.53922	0.08353
C	0.14055	-2.63066	-1.18620
C	0.37743	-3.99237	-1.85205
C	-1.35857	-2.48802	-0.92269
O	0.49155	-1.53799	-2.02950
C	1.88968	-1.39727	-2.20977
C	2.64851	-1.24260	-0.86571
C	4.14503	-1.36736	-1.22513
H	2.28715	1.35750	-1.96296
H	3.80256	1.39061	-1.08590
H	1.19877	2.81016	-0.40491
H	2.73500	3.52676	-0.85405

H	3.81643	4.51267	1.04869
H	3.69074	3.73154	2.72278
H	0.51593	3.02298	2.23083
H	-1.41974	2.09107	2.46482
H	0.01977	-0.75615	4.25306
H	-2.14315	-2.27757	4.33187
H	-1.05167	-2.93345	3.07609
H	4.72914	1.03847	0.87604
H	4.76362	-0.60702	1.48178
H	4.47884	0.69411	2.58601
H	1.16559	-1.04476	2.11292
H	2.57287	-0.98997	3.15988
H	2.26709	-3.15394	2.05048
H	3.78110	-2.45136	1.51751
H	1.43311	-4.17500	-2.07136
H	-0.15547	-4.06032	-2.80658
H	0.05023	-4.80856	-1.19852
H	-1.57630	-1.49259	-0.52523
H	-1.71149	-3.22178	-0.19014
H	-1.94026	-2.59177	-1.84512
H	2.05211	-0.53621	-2.86399
H	2.25916	-2.25882	-2.77900
H	4.47043	-0.56504	-1.89448
H	4.33715	-2.31033	-1.75265
H	4.80432	-1.37501	-0.36108

\*